A Neanderthal from the Central Western Zagros, Iran. Structural reassessment of the Wezmeh 1 maxillary premolar

Clément Zanolli, Fereidoun Biglari, Marjan Mashkour, Kamyar Abdi, Hervé Monchot, Karyne Debue, Arnaud Mazurier, Priscilla Bayle, Mona Le Luyer, Hélène Rougier, et al.

A Neanderthal from the Central Western Zagros, Iran. Structural reassessment of the Wezmeh 1 maxillary premolar

Clément Zanolli [a, *], Fereidoun Biglari [b, *], Marjan Mashkour [c, d], Kamyar Abdi [e], Hervé Monchot [f], Karyne Debue [c], Arnaud Mazurier [g], Priscilla Bayle [a], Mona Le Luyer [a, h], Hélène Rougier [i], Erik Trinkaus [j], Roberto Macchiarelli [k,l]

[a] *Laboratoire PACEA, UMR 5199 CNRS, Université de Bordeaux, Ministère de la Culture, Bordeaux, France*

[b] *Paleolithic Department, National Museum of Iran, Tehran, Iran*

[c] *Laboratoire AASPH, UMR 7209 CNRS, Muséum national d'Histoire naturelle, Paris, France*

[d] *Archaeozoology Section, Bioarchaeology Laboratory, Central Laboratory, University of Tehran, Tehran, Iran*

[e] *University of Shiraz, Shiraz, Iran*

[f] *UMR 8167 Orient et Méditerranée, Paris Sorbonne Universités, Paris, France*

[g] *Institut de Chimie des Milieux et Matériaux, UMR 7285 CNRS, Université de Poitiers, Poitiers, France*

[h] *Skeletal Biology Research Centre, School of Anthropology and Conservation, University of Kent, Canterbury, UK*

[i] *Department of Anthropology, California State University, Northridge, CA 91330, USA*

[j] *Department of Anthropology, Washington University, Saint Louis, MO 63130, USA*

[k] *Laboratoire HNHP, UMR 7194 CNRS, Muséum national d'Histoire naturelle, Musée de l'Homme, Paris, France*

[l] *Unité de Formation Géosciences, Université de Poitiers, Poitiers, France*

* Corresponding authors.

E-mail addresses: clement.zanolli@gmail.com (C. Zanolli), fbiglari@gmail.com (F. Biglari).

Acknowledgments

Research funded by the French CNRS. We thank the National Museum of Iran for research support, contribution and generous collaboration; the UMR 7209 for funding the surface scans at the SURFAçUS Platform of the MNHN Paris and the 3D print of Wezmeh 1; the PLATeforme INstrumentale d'Analyse of the IC2MP laboratory of the University of Poitiers for access to the μCT device; and the LabEx "Sciences archéologiques" of the University of Bordeaux for the analysis of comparative materials. We also thank the Editor, the Associate Editor, and the two anonymous reviewers for their helpful comments on the manuscript.

A Neanderthal from the Central Western Zagros, Iran. Structural reassessment of the Wezmeh 1 maxillary premolar

ABSTRACT

Wezmeh Cave, in the Kermanshah region of Central Western Zagros, Iran, produced a Late Pleistocene faunal assemblage rich in carnivorans along with a human right maxillary premolar, Wezmeh 1, an unerupted tooth from an 8 ± 2 year-old individual. Uranium-series analyses of the fauna by alpha spectrometry provided age estimates between 70 and 11 ka. Crown dimensions place the tooth specimen at the upper limits of Late Pleistocene human ranges of variation. Wezmeh 1 metameric position (most likely a P^3) remains uncertain and only its surficial morphology has been described so far. Accordingly, we used micro-focus X-ray tomography (12.5 μm isotropic voxel size) to reassess the metameric position and taxonomic attribution of this specimen. We investigated its endostructural features and quantified crown tissue proportions. Topographic maps of enamel thickness (ET) distribution were also generated, and semilandmark-based geometric morphometric analyses of the enamel-dentine junction (EDJ) were performed. We compared Wezmeh 1 with unworn/slightly-moderately worn P^3 and P^4 of European Neanderthals, Middle Paleolithic modern humans from Qafzeh, an Upper Paleolithic premolar, and Holocene humans. The results confirm that Wezmeh 1 represents a P^3. Based on its internal conformation and especially EDJ shape, Wezmeh 1 aligns closely with Neanderthals and is distinct from the fossil and extant modern human pattern of our comparative samples. Wezmeh 1 is thus the first direct evidence of Neanderthal presence on the western margin of the Iranian Plateau.

Keywords: Zagros Mountains; Wezmeh Cave; Human premolar tooth; Microfocus X-ray tomography; Neanderthals

1. Introduction

Since Coon's pioneering excavation in the late 1940s at the Middle Paleolithic site of Bisitun Cave (Coon, 1951), the Zagros Mountains of Iran and Iraq have produced a number of Late Pleistocene human remains associated with Middle and Upper Paleolithic technocultural contexts that represent the main bioanthropological source of information about the populations inhabiting the region during the oxygen isotope stages (OIS) 3–2 (for a recent chronometric assessment of some Middle and Upper Paleolithic sites of the region, see Becerra-Valdivia et al., 2017). Among the excavated sites yielding human remains, with its assemblage of at least ten Neanderthal individuals, the Shanidar Cave, Iraqi Kurdistan, has produced one of the largest sample of fossil human remains from Southwestern Asia thus far (Solecki, 1963; Trinkaus, 1983; Cowgill et al., 2007; Pomeroy et al., 2017).

A complex of Paleolithic sites in the Kermanshah region of Central Western Zagros, Iran, produced the second fossil human sample (Fig. 1). Among these sites, the Middle Paleolithic sequence of Bisitun Cave, located east-northeast of Kermanshah, was the first that yielded a human fossil (Coon, 1951), a right radius preserved from just distal of the radial tuberosity to the distal diaphysis. Although its dimensions overlap the upper end of the earlier Upper Paleolithic range of variation, comparisons with Neanderthal and Middle Paleolithic early modern human right radii align it predominantly with Neanderthals, but separate from Middle Paleolithic early modern humans of Southwestern Asia (Trinkaus and Biglari, 2006).

In the course of a reanalysis at the Field Museum of Natural History of the Upper Paleolithic collections from the Warwasi rockshelter, a site in the northern outskirt of Kermanshah, an isolated M_2 from a fossil modern human was recently identified in the faunal assemblage from the Baradostian levels (Tsanova, 2013).

Another Paleolithic site in Western Zagros that provided human remains is Gar Arjeneh, near Khoramabad, in Luristan. First excavated by Hole and Flannery (1967; for a review see Bazgir et al., 2014), its Baradostian levels have yielded a human premolar and some bone fragments (Trinkaus, 2018).

In the Southern Zagros, the Upper Paleolithic and Epipaleolithic layers of Eshkaft-e Gavi, near Shiraz, produced an assemblage of fragmentary dental, cranial and postcranial remains sampling a minimum of four modern human individuals bearing evidence of stone-tool cutmarks and burning (Rosenberg, 1985; Scott and Marean, 2009).

Finally, the catalog of human remains from Paleolithic sites of Central Western Zagros Mountains includes Wezmeh 1, an isolated maxillary premolar from Wezmeh Cave, southwest of Kermanshah. Its buccolingual crown diameter places it at the upper limits of Late Pleistocene human maxillary third (P^3) and fourth premolar (P^4) dimensions and above a terminal Pleistocene Natufian sample (Trinkaus et al., 2008).

Given uncertainties concerning the original chronostratigraphic context of Wezmeh 1 (Abdi et al., 2002; Trinkaus et al., 2008; Mashkour et al., 2009) and the difficulties of assessing its taxonomic status based on its external features (Trinkaus et al., 2008), we used micro-focus X-ray tomography (μCT) to reassess the metameric position and taxonomic attribution of this specimen. Using techniques of virtual imaging coupled with geometric morphometrics, we evaluated its tissue proportions, enamel thickness topographic distribution, enamel-dentine junction morphology, and pulp cavity shape. We then compared these data to samples of European Neanderthals, Near Eastern Middle Paleolithic modern humans, an Upper Paleolithic human, and Holocene humans.

1.1. The Wezmeh Cave

Wezmeh Cave is located 10 km southeast of the town of Islamabad-e Gharb (34°03'17.04" N, 46°38'41.03" E), at an elevation of ca. 1430 m asl (Fig. 1). The cave, discovered in 1999 during archeological survey as a part of the Islamabad Project (director: K.A.), is in a small valley in the western foothills of the Qazivand Mountain (Fig. 2a). Its entrance (Fig. 2b) faces north and is 2 m wide and 1.2 m high. The cave is about 27 m long and has about 45 m^2 of floor area (Abdi et al., 2002; see Fig. 2c). In 2001, following disturbance by clandestine digging, a 3 × 3 m trench was excavated to the bedrock on the terrace immediately outside of the cave entrance, and six small test pits at 2 m intervals were dug to bedrock within the cave. These excavations yielded Holocene (Chalcolithic) archeological materials (Abdi et al., 2002). The surface collecting on the exterior slope (Fig. 2b) in 1999, 2001 and 2008 yielded an abundant faunal assemblage, particularly rich in carnivoran and ungulate remains (Trinkaus et al., 2008; Mashkour et al., 2009). The faunal list includes carnivorans present during the Late Pleistocene in Southwest Asia: Hyenidae (*Crocuta crocuta*), Canidae (*Vulpes vulpes*, *Canis lupus*), Felidae (*Panthera leo*, *Panthera pardus*, *Caracal*/*Lynx*/*Felis chaus*, *Felis silvestris*), Mustelidae (*Meles meles*, *Martes martes*, *Mustela putorius*), Viverridae (*Herpestes* sp.), and Ursidae (*Ursus arctos*). Artiodactyl remains include Suidae (*Sus scrofa*), Cervidae (*Cervus elaphus*), Bovidae (*Bos primigenius*, *Gazella* sp., *Capra aegagrus*, *Ovis orientalis*). Among smaller taxa, representatives of Lagomorpha, Rodentia, Insectivora, and Reptilia were also found. The skeletal remains were mainly collected in disturbed late Pleistocene deposits and a small number from excavated early Holocene deposits. Three carnivoran coprolites from disturbed deposits were dated by ^{14}C (Djamali et al., 2011) to the Last Glacial Period (19,228 ± 352 cal yr BP and 12,744 ± 370 cal yr BP) and to the recent Holocene (405 ± 59 cal yr BP). Several fragmented human bones and teeth were discovered among the faunal remains, including the premolar Wezmeh 1 (Fig. 2d). A few other fragmented human bones and

96 teeth were also found in the cave; one of them was dated to the early Neolithic, at around 9300 cal
97 yr BP (Broushaki et al., 2016).
98 Because of the exceptional nature, size and taxonomic diversity of the assemblage from
99 Wezmeh Cave and the joint presence of extinct mammal taxa including human remains (notably
100 the large and fossilized tooth Wezmeh 1), a program of absolute dating of targeted specimens was
101 developed. According to uranium-series analyses of the fauna by alpha spectrometry, the site was
102 occupied by carnivorans within the interval 70–11 ka (OIS 4–2). The human premolar was directly
103 dated by gamma spectrometry to 25–20 ka (Trinkaus et al., 2008; Mashkour et al., 2009). However,
104 given that these dates are approximate and may be only minimum ages, Wezmeh 1 is currently
105 assigned to either OIS 3 or early OIS 2 (Trinkaus et al., 2008).
106
107 **2. Materials and methods**
108 Wezmeh 1 is an unerupted right upper premolar from an 8 ± 2 year-old individual (Trinkaus et
109 al., 2008; see Fig. 2c). The specimen consists of a finely preserved crown and of ca. 7 mm of
110 growing root (developmental stage between $R_{1/4}$ and $R_{1/2}$ following Moorrees et al., 1963), which
111 is largely complete up to its developing edge despite some local chipping.
112 The specimen was imaged at the University of Poitiers, France, using an EasyTom XL Duo
113 device (RX-Solutions) set at the PLATINA platform of the IC2MP laboratory. A sealed
114 Hamamatsu microfocus X-ray source (small focal spot mode) was used, coupled to a Varian
115 PaxScan 2520DX imager. The acquisition parameters are: 60kV voltage; 166 µA current; a 0.35
116 mm Cu filter; 1280 projections, 4 frames/second; averaging of 13 frames/projection; anti-ring shift
117 procedure; source-to-detector distance and source-to-object distance of 416 mm and 41 mm,
118 respectively, and reconstructed with a voxel size of 12.5 µm. Reconstruction of the data was done
119 with the XAct software (RX-solutions) with a filtered back projection algorithm (Felkamp method

for cone beam geometry with a Tukey filter) and correction of beam hardening artefacts through linearization with a polynomial function. A semiautomatic threshold-based segmentation was conducted using Avizo v.8.0 (FEI Visualization Sciences Group, Hillsboro), following an adaptation of the half-maximum height method (Spoor et al., 1993; Fajardo et al., 2002; Coleman and Colbert, 2007). The crown was virtually isolated from the roots (Olejniczak et al., 2008) and 3D surface models of the dental tissues were generated using a constrained smoothing algorithm (Kupczik and Hublin, 2010).

For assessing tissue proportions, the following variables were measured on the 2D buccolingual virtual tooth section (Feeney et al., 2010) and calculated in 3D (see Kono, 2004; Macchiarelli et al., 2006; Olejniczak et al., 2008; Bayle et al., 2010; Smith et al., 2012; Skinner et al., 2015): enamel area (c; mm^2); coronal dentine and pulp area (b; mm^2); total crown area (a; mm^2); percentage of crown area that is dentine and pulp (b/a; %); enamel-dentine junction (EDJ) length (e; mm); bicervical diameter (BCD; mm); enamel volume (Ve; mm^3); coronal dentine and pulp volume (Vcdp; mm^3); total crown volume (Vc; mm^3); percentage of crown volume that is dentine and pulp (Vcdp/Vc; %); EDJ surface area (SEDJ; mm^2). Enamel thickness was assessed by calculating the following parameters (Martin, 1985; Olejniczak et al., 2008): 2D average enamel thickness (2D AET = c/e; mm) and 2D relative enamel thickness (2D RET = 2D AET*100/($b^{1/2}$); scale-free); 3D average enamel thickness (3D AET = Ve/SEDJ; mm) and 3D relative enamel thickness (3D RET = 3D AET*100/($Vcdp^{1/3}$); scale-free).

Three-dimensional maps of topographic enamel thickness distribution were created with the segmented enamel and crown dentine components (Macchiarelli et al., 2008; Bayle et al., 2011; Zanolli et al., 2018a, b), where differences in enamel distribution are rendered by a thickness-related pseudocolor scale ranging from dark blue (thinner) to red (thicker). This method maps topographic thickness variation at the outer enamel surface and facilitates the site-specific and

144 synthetic comparative assessments of this feature. The topographic variation of standardized
145 enamel thickness was measured using MPSAK v2.9 (available in Dean and Wood, 2003) in the
146 lingual and buccal aspects of the virtual buccolingual section (Macchiarelli et al., 2007; Le Luyer
147 and Bayle, 2017), and the values were calibrated with respect to a bicervical diameter of 6 mm
148 (Schwartz, 2000; Mazurier et al., 2003; Le Luyer, 2016).

149 Geometric morphometric (GM) analyses of EDJ were performed on the virtual surface by
150 placing two landmarks at the apices of the paracone and protocone dentine horns and 71
151 semilandmarks along the marginal ridges (33 on the mesial marginal ridge and 38 on the distal
152 one). We performed the generalized Procrustes analyses, followed by between-group principal
153 component analyses (bgPCA) and Jackknife cross-validated canonical variate analyses (CVA)
154 based on the first 9 (for the separate P^3 and P^4 samples) to 12 (for the combined P^3–P^4 samples)
155 first principal components explaining ~90% of the total variance (Mitteroecker and Bookstein,
156 2011; Krenn et al., 2019). Wezmeh 1 was included a posteriori in the analyses. Multivariate
157 analyses were performed using the packages ade4 v.1.7-6 (Dray and Dufour, 2007) and Morpho v.
158 2.7 (Schlager, 2019) for R v.3.6 (R Development Core Team, 2019). Allometry was tested using
159 the coefficient of determination (R^2) of a multiple regression (Bookstein, 1991) in which the
160 explicative variable is the centroid size and the dependent variables are the bgPC scores (see also
161 Mitteroecker et al., 2013).

162 Because of the uncertainty of the Wezmeh 1 metameric position, the comparative analyses used
163 the μCT record of selected unworn/slightly-moderately worn crowns (wear stage ≤ 2 following
164 Smith, 1984) of both P^3 and P^4 representing: European Neanderthals (NEA) from Krapina, Sima
165 de las Palomas, and Spy (Bayle et al., 2017, In press; NESPOS Database, 2019); Middle Paleolithic
166 modern humans (MPMH) from Qafzeh (Qafzeh 10 and 15 [ESRF, 2019] and Qafzeh 4 [original
167 data]), and Holocene humans (HH) of Western European origin (Le Luyer, 2016 and original data).

168 Due to the limited μCT-based comparative evidence directly available to us or exploitable from
169 the literature, the fossil modern human sample (MPMH) is restricted to the material from the site
170 of Qafzeh, thus resulting in a temporal and geographic gap between the fossil and recent
171 comparative samples. However, we also exploited the endostructural signal from an unpublished
172 late Upper Paleolithic (Magdalenian) P^3 from the French site of La Piscine (see Discussion and
173 conclusions), suggesting that this heterogeneous sample is still representative of the fossil modern
174 human variation. Information on the three comparative samples (including the variable number of
175 cases used in the different 2-3D analyses) is reported in Table 1, while Table 2 provides the NEA
176 and MPMH samples. The sample of Holocene premolars used in this study, consisting of
177 archaeological and recent specimens from Western Europe, is provided in Supplementary Online
178 Material (SOM) Table S1.
179 In a few cases, local virtual integrations of the outer enamel surface and/or of the dentine horn
180 tip contour were made preliminary to the quantitative analyses on 2D virtual sections and 3D
181 models, respectively. Within each sample, integration of the removed enamel was based on the
182 preserved morphology of the unworn crowns as revealed by their serial buccolingual cross-sections
183 (Smith et al., 2012).
184 Adjusted Z-scores (Maureille et al., 2001; Scolan et al., 2012) were computed to compare the
185 3D dental tissue proportions and enamel thickness values of Wezmeh 1 to the means and standard
186 deviations of the comparative groups. This method allows the comparison of unbalanced samples,
187 which is often the case when dealing with the fossil record, by using the Student's t inverse
188 distribution, where the +1.0 to -1.0 interval comprises 95% of the variation in the reference sample.
189 Plots of the common logarithm (log) of 2D AET against the log of coronal dentine and pulp area
190 (b) were used to illustrate the relationship between AET and tooth size (Skinner et al., 2015) and
191 to show the placement of Wezmeh 1 compared to Neanderthals, MPMH and Holocene humans.

For the GM assessment of the EDJ morphology, Wezmeh 1 was projected a posteriori in the bgPCA analysis.

3. Results

The virtual reconstructions of the outer enamel surface (OES) and of the internal aspect of Wezmeh 1 in different views are comparatively shown in Figure 3. The specimen exhibits excellent preservation of its outer and inner morphology. It also lacks sedimentary infill and displays high enamel-dentine contrast in all μCT-based reconstructions.

On the lateral and occlusal aspects, the undamaged and unworn OES shows several small and shallow pits representing minor developmental enamel defects. However, these hypoplastic defects are not visible on the EDJ (Fig. 3). Otherwise, the OES and the dentine surface morphology match perfectly. Specifically, in occlusal view, they share: a low elevation of the buccal segment of the mesial marginal ridge, with a short crest running into the mesial fovea; two buccal and two lingual essential segments of the bifurcated transverse crest; a short distal crest running from the lingual cusp; and a small cusp-like elevation visible on the lingual part of the distal marginal ridge (Fig. 3).

Near the cervix, a shallow subcircular enamel depression is noticeable on the mesiobuccal aspect of the paracone. The virtual rendering of the coronal dentine shows that its imprint is also slightly expressed beneath the enamel (Fig. 3). Approximately 2.0 mm from the cervix, this feature also extends to the root dentine (Trinkaus et al., 2008), where it appears as a larger and deeper depression (Fig. 3; SOM Fig. S1). Apparently, it does not affect the pulp morphology, the inner dentine wall being straight and flat at the level of the depression, even if the dentine at this spot is thinner than measured at other points of the growing root (SOM Fig. S1).

2D and 3D measures of crown tissue proportions and enamel thickness in Wezmeh 1 are reported in Tables 3 and 4, respectively, together with the comparative estimates for each premolar type of the NEA, MPMH, and HH samples used in this study.

For a large majority of the measured/calculated parameters, the values (absolute and proportions) displayed by the P^3 and P^4 crowns overlap within each sample, or are close. A greater variation characterizes the MPMH sample, especially for b/a, 2D RET, Vcdp/Vc, SEDJ, and 3D RET. Whatever its metameric position, Wezmeh 1 shows absolutely higher values for most of the 2D and 3D tissue proportion parameters. It fits better with the Neanderthal P^3 and, to a slightly lesser extent, the Neanderthal P^4. The variables that align the Iranian specimen and the Neanderthals and best discriminate both from the fossil and recent modern human figures are: c, b, e, Ve, Vcdp, and SEDJ (Tables 3 and 4). For these parameters, Wezmeh 1 is clearly apart from the HH condition and approaches the NEA pattern, while the MPMH tend to occupy an intermediate position between the HH and NEA values. However, no substantial differences exist between Wezmeh 1 and the comparative samples for b/a and Vcdp/Vc, notably among the P^3. Whatever the extent of the differences shown in Tables 3 and 4, all of the comparisons with the MPMH and HH representatives show that the whole inner structural signature of Wezmeh 1 better fits those expressed by the P^3, not the P^4.

A closer affinity of Wezmeh 1 with the Neanderthals is revealed by the adjusted Z-scores of the absolute estimates of nearly all 2D and 3D variables (SOM Figs. S2 and S3). However, this is not the case for the enamel thickness. In fact, for both 2D and 3D AET, Wezmeh 1 is compatible with the HH values. Nonetheless, for both size-free 2D and 3D RET indices, the Iranian tooth crown is slightly closer to the NEA estimates (Tables 3 and 4). Additionally, the affinity of Wezmeh 1 with NEA is shown by the bivariate graph of log 2D AET against log b (Fig. 4), which also includes

two specimens from Qafzeh and where Wezmeh 1 plots among the NEA specimens and apart from the HH by having larger coronal dentine and pulp areas.

The cartographies of enamel thickness distribution in Wezmeh 1 and in representatives of the comparative samples (NEA, MPMH and HH) are shown in Figures 5 and 6, separately for the P^3 and P^4 crowns imaged in different projections. As a whole, they reveal only minor differences among the investigated specimens, including between NEA and HH. At least in the limited comparative assemblage of premolar crowns available, it appears that the relatively thicker Qafzeh 4 specimen, similar to the HH P^3, exhibits thicker enamel distributed over the occlusal basin and at the cusp apices, especially the protocone, whereas in the relatively thinner Qafzeh 10, thicker enamel is mostly localized on the protocone, as in NEA. Nonetheless, Wezmeh 1 shares with Qafzeh 4 and NEA P^3, a relatively thicker enamel on the buccal aspect.

A more detailed picture illustrating topographic enamel thickness variation is shown by the site-specific standardized values comparatively assessed from the cervix towards the apex across the entire lingual (protocone) and buccal (paracone) mesiodistal virtual sections, respectively (SOM Figs. S4 and S5). The enamel distribution in Wezmeh 1 follows the NEA pattern revealed by the pooled P^3 and P^4, especially for the lingual cross-section (SOM Fig. S4). Conversely, for the buccal section, its trajectory is less distinct, including when compared to the MPMH and the HH pattern. In this respect, Wezmeh 1's profile follows a modern-like trajectory along approximately the first half of its buccal section and a Neanderthal-like trajectory nearing the paracone (SOM Fig. S5).

The results of the bgPCA of the geometric morphometric analysis of the EDJ in the shape space of the P^3 and P^4 are displayed in Fig. 7. The first two components, which account for 88.6% of the total variation (59.8% for bgPC1 and 31.5% for bgPC2), show a weak allometric signal ($p < 0.05$; $R^2 = 0.34$) and no size-dependent shape variation ($p > 0.05$; $R^2 = 0.06$). The GM analysis combining P^3 and P^4 thus mostly represents shape variation. By displaying a relatively symmetrical outline of

262 the occlusal basin and a large distal part of the occlusal basin, Wezmeh 1 falls within the NEA P^3
263 variation space. It is also relatively close to the NEA P^4 shape, a space characterized by a slightly
264 more reduced talon, as well as by an acute mesiobuccal angle of the occlusal basin. In this context,
265 the Iranian tooth differs from the upper premolars from Qafzeh by having a more symmetrical
266 outline of the EDJ, and is also well separated from the HH P^3 and P^4 by having a more mesiodistally
267 extended talon and a more marked distolingual extension of the latter. These results are confirmed
268 by the CVA, in which the predictive accuracy between human groups is robust (100% correct
269 classification for NEA, 83.3% for MPMH, and 96.3% for HH), and the Iranian specimen is
270 classified with 100% posterior probability as NEA. We also ran a CVA to assess metameric
271 variation in the comparative sample (predictive accuracy: 88.5% and 87.5% of correct
272 classification for P^3 and P^4, respectively). This analysis indicates a 100% posterior probability of
273 Wezmeh 1 representing a P^3.

274 We also analyzed Wezmeh 1 separately with the P^3 (SOM Fig. S6) and the P^4 (SOM Fig. S7).
275 Again, only a weak allometric signal is found along the bgPC1 ($R^2 = 0.48$ and 0.34 for the P^3 and
276 the P^4 analyses, respectively), while no allometry is recorded along the bgPC2 for both analyses (p
277 > 0.05; $R^2 < 0.03$). When compared with the P^3, Wezmeh 1 is much closer to the NEA condition
278 than to the MPMH and HH groups. More specifically, the Iranian premolar exhibits the typical
279 Neanderthal square outline of the occlusal basin, whereas the other groups have a more ovoid
280 pattern (SOM Fig. S6). Compared with the P^4 (SOM Fig. S7), Wezmeh 1 again fits the NEA shape
281 and sets apart from both the three MPMH (displaying a more rounded outline of the occlusal basin)
282 and the HH sample (characterized by a shorter talon and no angulation of the distolingual corner).
283

284 **4. Discussion and conclusions**

A number of sites in Central and Southern Zagros have yielded variably rich Mousterian lithic assemblages (e.g., Biglari, 2007; Otte et al., 2009; Scott and Marean, 2009; Bazgir et al., 2014, 2017; Shidrang et al., 2016; Becerra-Valdivia et al., 2017; Heydari-Guran and Ghasidian, 2017). Within an approximate 30 km radius of Wezmeh Cave, 13 Middle Paleolithic sites have been recorded; among them, the nearest sites (cluster of Cham Souran and Cham Barzeh) are located about 10 km to the northwest (Biglari and Abdi, 1999). Surface collected lithic artifacts from these cave, rockshelter and open-air sites generally resemble excavated Zagros Mousterian assemblages from sites situated in the neighboring intermountain plain of Kermanshah. However, the physical record of their producers remains elusive (review in Trinkaus, 2018).

The first description of the isolated immature human upper premolar Wezmeh 1 suggested it more likely represents a P^3 (Trinkaus et al., 2008). Our comparative observations combining outer morphology and inner structural organization corroborate this attribution. Importantly, the new analyses add relevant information to more confidently assess the taxonomic status of this specimen. Even if the possibility that Wezmeh 1 "could derive from an earlier OIS 3 Neandertal" (Trinkaus et al., 2008: 376) was evoked because of its large buccolingual crown diameter, based solely on its outer crown characteristics, its attribution to a late archaic or an early modern human was unclear (Trinkaus et al., 2008). However, our analyses of the internal structure confirm that Wezmeh 1 belongs to a Neanderthal.

Because of its discriminant value, quantitative information on the inner tooth structural organization and tissue proportions is increasingly used in paleoanthropological research as a reliable tool of taxonomic significance, including among species within the genus *Homo* (e.g., Macchiarelli et al., 2006; Olejniczak et al., 2008; Skinner et al., 2008; Smith et al., 2009; Bayle et al., 2010; Benazzi et al., 2011; Liu et al., 2013; Crevecoeur et al., 2014; Martinón-Torres et al.,

2014; Weber et al., 2016; Hublin et al., 2017; Martin et al., 2017; Martínez de Pinillos et al., 2017; Pan et al., 2017; Hershkovitz et al., 2018; Xing et al., 2018; Zanolli et al., 2018a).

Our μCT-based analyses indicate that the Iranian premolar most likely derives from a Neanderthal-like individual to a degree of reliability comparable to that usually accepted for discriminating Neanderthal from extant and fossil modern human molar teeth (e.g., Olejniczak et al., 2008; Smith et al., 2012; Weber et al., 2016; Bayle et al., 2017; Martin et al., 2017; Zanolli et al., 2018a). In this context, the results of the 3D geometric morphometric analysis of the EDJ conformation are of special value, as EDJ topography approximates the inner enamel epithelium of the developing tooth and provides useful information about taxon-specific processes underlying crown growth (e.g., Skinner et al., 2008; Crevecoeur et al., 2014; Zanolli, 2015; Martin et al., 2017; Zanolli et al., 2019).

Studies of the outer crown morphology indicate that there are no particular non-metric features enabling to diagnostically attribute an isolated upper premolar to a Neanderthal or to an early modern human (e.g., Bailey, 2006; Bailey and Hublin, 2013). However, the bifurcated essential crest slightly visible in Wezmeh 1, notably at the EDJ level, is generally present in Neanderthals but, to the best of our knowledge, has not been recorded in early modern humans thus far (Bailey, 2006), evidence that strengthens our endostructurally-based attribution of Wezmeh 1 to a Neanderthal individual.

Besides the limited size of the available comparative fossil samples, information currently is rare for coronal tissue proportions and enamel thickness variation of upper premolar crowns, including in recent humans (Feeney et al., 2010; Le Luyer, 2016). Importantly for this study, no data suitable for direct comparisons have been published so far on tooth tissue proportions of fossil modern human P^3. The μCT record of an unpublished right P^3 (specimen H3) from the Magdalenian (OIS 2) site of La Piscine, in Montmorillon, Central-Western France (Henry-

Gambier, 2010; Delage, 2011), allowed us to use this otherwise worn tooth (stage 4) for the GM-based comparative analysis of the EDJ. Following a virtual integration of its slightly eroded protocone (SOM Fig. S8a)—according to the geometric method described in Zanolli et al. (2018a)—the bgPCA results (SOM Fig. S8b) show that this latest Pleistocene tooth plots together with the MPMH P^3, distant from Wezmeh 1.

In our analyses, a Neanderthal vs. modern human-like signature is less distinct for the enamel thickness, whatever the parameter used. The absolute enamel volume of Neanderthal upper and lower molars is comparable to that of modern humans, but in Neanderthals it is deposited over a larger volume of coronal dentine, thus resulting in lower average and relative enamel thickness values (Olejniczak et al., 2008). However, the possibility exists that enamel thickness in upper premolars is not as powerful to discriminate between Neanderthals and modern humans. This hypothesis should be tested in larger samples. Unfortunately, no directly comparable quantitative information on the inner tooth structural organization and topographic enamel thickness variation is available so far on Neanderthal premolars from Southeast Asia.

An additional limiting aspect in our study is the fact that Wezmeh 1 is from a still growing individual bearing a modest portion of radicular dentine (Trinkaus et al., 2008). This prevents the possibility of virtually unrolling and projecting it into a standardized morphometric map for assessing its topographic thickness variation, a feature which tends to discriminate Neanderthal from non-Neanderthal teeth (e.g., Bayle et al., 2010; Bondioli et al., 2010; Macchiarelli et al., 2013; Zanolli et al., 2014, 2018a).

As first noted by Trinkaus et al. (2008), an interesting feature in Wezmeh 1 is represented by a distinct depression located on its mesial root aspect. In this study we investigated its occurrence in two comparative P^3 and P^4 samples representing 20 Western European Neanderthals (Rougier, 2003; Toussaint, 2014; NESPOS Database, 2019) and 48 Western European Holocene humans (Le

Luyer, 2016 and original data; SOM Table S2). According to our record, a similar and topographically homologous feature occurs more frequently on the P^3, either in Neanderthals (7/12) or extant humans (7/28), whereas it is rarely present on the P^4 (1/8 and 0/20, respectively). Additionally, at least among the samples available to us, this radicular depression is more frequent in European Neanderthals (8/18) than in Holocene humans (7/48). However, further studies are necessary to elucidate its nature and significance as a possible taxon/population-related feature.

Along with the Shanidar remains from further north, the Wezmeh 1 maxillary premolar, from the Central Western Zagros of Iran, provides solid evidence for the presence of Neanderthals through the Zagros Mountains in the Late Pleistocene. Although undated other than to at least OIS 3, or OIS 2 (Trinkaus et al., 2008), its morphological affinities and the presence of a Late Pleistocene faunal assemblage from Wezmeh Cave (Mashkour et al., 2009) strongly imply that it derives from the earlier OIS 3 and therefore relates to the increasingly documented Middle Paleolithic of the region. As such, it adds to the limited evidence for Neanderthals in Southwest Asia east of the Mediterranean region.

References

Abdi, K., Biglari, F., Heydari, S. 2002. Islamabad Project 2001. Test excavations at Wezmeh cave. Archäologische Mitteilungen aus Iran und Turan 34, 171-194.

Bailey, S.E., 2006. Beyond shovel-shaped incisors: Neandertal dental morphology in a comparative context. Periodicum Biologorum 108, 253-267.

Bailey, S.E., Hublin, J.-J., 2013. What does it mean to be dentally "modern"? In: Scott, G.R., Irish, J.D. (Eds.), Anthropological Perspectives on Tooth Morphology. Genetics, Evolution, Variation. Cambridge University Press, Cambridge, pp. 222-249.

Bayle, P., Bondioli, L., Macchiarelli, R., Mazurier, A., Puymerail, L., Volpato, V., Zanolli, C., 2011. Three-dimensional imaging and quantitative characterization of human fossil remains. Examples from the NESPOS database. In: Macchiarelli, R., Weniger, G.-C. (Eds.), Pleistocene Databases. Acquisition, Storing, Sharing. Wissenschaftliche Schriften des Neanderthal Museums 4, 29-46.

Bayle, P., Le Luyer, M., Robson Brown, K.A., 2017. The dental remains: Enamel thickness, and tissue proportions. In: Trinkaus, E., Walker, M.J. (Eds.), The People of Palomas: Neandertals from the Sima de las Palomas, Cabeza Gordo, Southeastern Spain. Texas A&M University Press, College Station, pp. 115-137.

Bayle, P., Macchiarelli, R., Trinkaus, E., Duarte, C., Mazurier, A., Zilhão, J., 2010. Dental maturational pattern and dental tissue proportions in the early Upper Paleolithic child from Abrigo do Lagar Velho, Portugal. Proceedings of the National Academy of Sciences USA 107, 1338-1342.

Bayle, P., Mazurier, A., Macchiarelli, R., In press. The permanent “virtual dentition”. In: Rougier, H., Semal, P. (Eds.), Spy Cave. 125 Years of Multidisciplinary Research at the Betche aux Rotches (Jemeppe-sur-Sambre, Province of Namur, Belgium), Volume 2. Anthropologica et Praehistorica 124/2013, Royal Belgian Institute of Natural Sciences, Royal Belgian Society of Anthropology and Praehistory & NESPOS Society, Brussels.

Bazgir, B., Ollé, A., Tumung, L., Becerra-Valdivia, L., Douka, K., Higham, T., van der Made, J., Picin, A., Saladié, P., López-García, J.M., Blain, H.-A., Allué, E., Fernández-García, M., Rey-Rodríguez, I., Arceredillo, D., Bahrololoumi, F., Azimi, M., Otte, M., Carbonell, E., 2017. Understanding the emergence of modern humans and the disappearance of Neanderthals: Insights from Kaldar Cave (Khorramabad Valley, Western Iran). Scientific Reports 7, 43460.

Bazgir, B., Otte, M. Tumung, L., Ollé, A., Deo, S.G., Joglekar, P., López-García, J.M., Picin, A., Davoudi, D., van der Made, J., 2014. Test excavations and initial results at the Middle and Upper Paleolithic sites of Gilvaran, Kaldar, Ghamari caves and Gar Arjene Rockshelter, Khorramabad Valley, western Iran. Comptes Rendus Palevol 13, 511-525.

Becerra-Valdivia, L., Douka, K., Comeskey, D., Bazgir, B., Conard, N.J., Marean, C.W., Ollé, A., Otte, M., Tumung, L., Zeidi, M., Higham, T.F.G., 2017. Chronometric investigations of the Middle to Upper Paleolithic transition in the Zagros Mountains using AMS radiocarbon dating and Bayesian age modelling. Journal of Human Evolution 109, 57-69.

Benazzi, S., Douka, K., Fornai, C., Bauer, C.C., Kullmer, O., Svoboda, J., Pap, I., Mallegni, F., Bayle, P., Coquerelle M., Condemi, S., Ronchitelli, A., Harvati, K, Weber, G.W., 2011. Early dispersal of modern humans in Europe and implications for Neanderthal behaviour. Nature 479, 525-528.

Biglari, F., 2007. Approvisionnement et utilisation des matières premières au Paléolithique moyen dans la plaine de Kermanshah (Iran): le cas de la Grotte Do-Ashkaft. In: Moncel, M.H., Moigne, A.-M., Arzarello, M., Peretto, C. (Eds), Aires d'Approvisionnement en Matières Premières et Aires d'Approvisionnement en Ressources Alimentaires. Approche Intégrée des Comportements. Proceedings of the XV UISPP World Congress (Lisbon, 4-9 September 2006), vol. 5. Archaeopress, Oxford.

Biglari, F., Abdi, K., 1999. Paleolithic artifacts from Cham-e Souran, the Islamabad Plain, Central Western Zagros Mountains, Iran. Archaologische Mitteilungen aus Iran und Turan 31, 1-8.

Bondioli, L., Bayle, P., Dean, C., Mazurier, A., Puymerail, L., Ruff, C., Stock, J.T., Volpato, V., Zanolli, C., Macchiarelli, R., 2010. Morphometric maps of long bone shafts and dental roots for imaging topographic thickness variation. American Journal of Physical Anthropology 142, 328-334.

426 Bookstein, F.L., 1991. Morphometric Tools for Landmark Data: Geometry and Biology.
427 Cambridge University Press, Cambridge.
428 Broushaki, F., Thomas, M.G., Link, V., López, S., van Dorp, L., Kirsanow, K., Hofmanová, Z.,
429 Diekmann, Y., Cassidy, L. M., Díez-del-Molino, D., Kousathanas, A., Sell, C., Robson, H.,
430 Martiniano, R., Blöcher, J., Scheu, A., Kreutzer, S., BollonginoR., Bobo, D., Davudi, H.,
431 Munoz, O., Currat, M., Abdi, K., Biglari, F., Craig, O. E., Bradley, D.G., Shennan, S.,
432 Veeramah, K.R., Mashkour, M., Wegmann, D., Hellenthal, G., Burger, J., 2016. Early Neolithic
433 genomes from the eastern Fertile Crescent. Science 353, 499-503.
434 Coleman, M.N., Colbert, M.W., 2007. Technical note: CT thresholding protocols for taking
435 measurements on three-dimensional models. American Journal of Physical Anthropology 133,
436 723-725.
437 Coon, C.S., 1951. Cave Explorations in Iran 1949. University of Pennsylvania, Philadelphia.
438 Cowgill, L.W., Trinkaus, E., Zeder, M.A., 2007. Shanidar 10: A Middle Paleolithic immature distal
439 lower limb from Shanidar Cave, Iraqi Kurdistan. Journal of Human Evolution 53, 213-223.
440 Crevecoeur, I., Skinner, M.M., Bailey, S.E., Gunz, P., Bortoluzzi, S., Brooks, A.S., Burlet, C.,
441 Cornelissen, E., De Clerck, N., Maureille, B., Semal, P., Vanbrabant, Y., Wood, B.A., 2014.
442 First early hominin from Central Africa (Ishango, Democratic Republic of Congo). PLoS One
443 9, e84652.
444 Dean, M.C., Wood, B., 2003. A Digital Radiographic Atlas of Great Apes Skull and Dentition. In:
445 Bondioli, L., Macchiarelli, R. (Eds.), Digital Archives of Human Paleobiology, 3. ADS
446 Solutions, Milano (CD-ROM).
447 Delage, C., 2011. Le Site Préhistorique de La Piscine, Montmorillon (Vienne), Volume 1.
448 Historique des Recherches (1966-1982). Les Editions du Musée de Montmorillon,
449 Montmorillon.

450 Djamali, M., Biglari, F., Abdi, K., Andrieu-Ponel, V., de Beaulieu, J-L., Mashkour, M., Ponel, P.,
451 2011. Pollen analysis of coprolites from a late Pleistocene-Holocene cave deposit (Wezmeh
452 Cave, west Iran): Insights into the late Pleistocene and late Holocene vegetation and flora of the
453 central Zagros Mountains. Journal of Archaeological Science 38, 3394-3401.
454 ESRF (European Synchrotron Radiation Facility), 2019. ESRF Paleontological Microtomographic
455 Database. http://paleo.esrf.eu.
456 Fajardo, R.J., Ryan, T.M., Kappelman, J., 2002. Assessing the accuracy of high-resolution X-ray
457 computed tomography of primate trabecular bone by comparisons with histological sections.
458 American Journal of Physical Anthropology 118, 1-10.
459 Feeney, R.N.M., Zermeno, J.P., Reid, D.J., Nakashima, S., Sano, H., Bahar, A., Hublin, J.-J.,
460 Smith, T.M., 2010. Enamel thickness in Asian human canines and premolars. Anthropological
461 Science 118, 191-198.
462 Henry-Gambier, D., 2010. Les fossiles humains du Paléolithique supérieur de Poitou-Charentes.
463 In: Buisson-Catil, J., Primault, J. (Eds.), Préhistoire entre Vienne et Charente. Hommes et
464 Sociétés du Paléolithique. Association des Publications Chauvinoises, Chauvigny, pp. 25-43.
465 Hershkovitz, I., Weber, G.W., Quam, R., Duval, M., Grün, R., Kinsley, L., Ayalon, A., Bar-
466 Matthews, M., Valladas, H., Mercier, N., Arsuaga, J.L., Martinón-Torres, M., Bermúdez de
467 Castro, J.M., Fornai, C., Martín-Francés, L., Sarig, R., May, H., Krenn, V.A., Slon, V.,
468 Rodríguez, L., García, R., Lorenzo, C., Carretero, J.M. Frumkin, A., Shahack-Gross, R., Bar-
469 Yosef Mayer, D.E., Cui, Y., Wu, X., Peled, N., Groman-Yaroslavski, I., Weissbrod, L.,
470 Yeshurun, R., Tsatskin, A., Zaidner, Y., Weinstein-Evron, M., 2018. The earliest modern
471 humans outside Africa. Science 359, 456-459.
472 Heydari-Guran, S., Ghasidian, E., 2017. The MUP Zagros Project: Tracking the Middle-Upper
473 Palaeolithic transition in the Kermanshah region, west-central Zagros, Iran. Antiquity 91, 1-7.

Hole, F., Flannery, K.V., 1967. The prehistory of Southwestern Iran: A preliminary report. Proceedings of the Prehistoric Society 22, 147-206.

Hublin, J.-J., Ben-Ncer, A., Bailey, S.E., Freidline, S.E., Neubauer, S., Skinner, M.M., Bergmann, I., Le Cabec, A., Benazzi, S., Harvati, K., Gunz, P., 2017. New fossils from Jebel Irhoud, Morocco and the pan-African origin of *Homo sapiens*. Nature 546, 289-292.

Kono, R., 2004. Molar enamel thickness and distribution patterns in extant great apes and humans: New insights based on a 3-dimensional whole crown perspective. Anthropological Science 112, 121-146.

Krenn, V.A., Fornai, C., Wurm, L., Bookstein, F.L., Haeusler, M., Weber, G.W., 2019. Variation of 3D outer and inner crown morphology in modern human mandibular premolars. American Journal of Physical Anthropology. https://doi.org/10.1002/ajpa.23858.

Kupczik, K., Hublin, J.J., 2010. Mandibular molar root morphology in Neanderthals and Late Pleistocene and recent *Homo sapiens*. Journal of Human Evolution 59, 525-541.

Le Luyer, M., 2016. Évolution dentaire dans les populations humaines de la fin du Pléistocène et du début de l'Holocène (19000-5500 cal. BP): une approche intégrée des structures externe et interne des couronnes pour le Bassin Aquitain et ses marges. Ph.D. Dissertation, Université de Bordeaux.

Le Luyer, M., Bayle, P., 2017. Microevolution of outer and inner structures of upper molars in Late Pleistocene and Early Holocene humans. In: Macchiarelli, R., Zanolli, C. (Eds.), Hominin Biomechanics, Virtual Anatomy and Inner Structural Morphology: From Head to Toe. A Tribute to Laurent Puymerail. Comptes Rendus Palevol 16, 632-644.

Liu, W., Shepartz, L.A., Xing, S., Miller-Antonio, S., Wu, X., Trinkaus, E., Martinón-Torres, M., 2013. Late Middle Pleistocene hominin teeth from Panxian Dadong, South China. Journal of Human Evolution 64, 337-355.

498 Macchiarelli, R., Bayle, P., Bondioli, L., Mazurier, A., Zanolli, C., 2013. From outer to inner
499 structural morphology in dental anthropology. The integration of the third dimension in the
500 visualization and quantitative analysis of fossil remains. In: Scott, R.G., Irish, J.D. (Eds.),
501 Anthropological Perspectives on Tooth Morphology: Genetics, Evolution, Variation.
502 Cambridge University Press, Cambridge, pp. 250-277.
503 Macchiarelli, R., Bondioli, L., Debénath, A., Mazurier, A., Tournepiche, J.-F., Birch, W., Dean,
504 M.C., 2006. How Neanderthal molar teeth grew. Nature 444, 748-751.
505 Macchiarelli, R., Bondioli, L., Mazurier, A., 2008. Virtual dentitions: Touching the hidden
506 evidence. In: Irish, J.D., Nelson, G.C. (Eds.), Technique and Application in Dental
507 Anthropology. Cambridge University Press, Cambridge, pp. 426-448.
508 Macchiarelli, R., Mazurier, A., Volpato, V., 2007. L'apport des nouvelles technologies à l'étude
509 des Néandertaliens. In: Vandermeersch, B., Maureille, B. (Eds), Les Néandertaliens. Biologie
510 et Cultures. C.T.H.S., Paris, pp. 169-179.
511 Martin, L.B., 1985. Significance of enamel thickness in hominoid evolution. Nature 314, 260-263.
512 Martin, M.R.G., Hublin, J-J, Gunz, P, Skinner, M.M., 2017. The morphology of the enamel-dentine
513 junction in Neanderthal molars: Gross morphology, non-metric traits, and temporal trends.
514 Journal of Human Evolution 103, 20-44.
515 Martínez de Pinillos, M., Martinón-Torres, M., Martín-Francés, L., Arsuaga, J.L., Bermúdez de
516 Castro, J.M., 2017. Comparative analysis of the trigonid crests patterns in *Homo antecessor*
517 molars at the enamel and dentine surfaces. Quaternary International 433, 189-198.
518 Martinón-Torres, M., Martínez de Pinillos, M., Skinner, M.M., Martín-Francés, L., Gracia-Téllez,
519 A., Martínez, I., Arsuaga, J.L., Bermúdez de Castro, J.M., 2014. Talonid crests expression at
520 the enamel-dentine junction of hominin lower permanent and deciduous molars. Comptes
521 Rendus Palevol. 13, 223-234.

522 Mashkour, M., Monchot, H., Trinkaus, E., Reyss, J.L., Biglari, F., Bailon, S., Heydari, S., Abdi,
523 K., 2009. Carnivores and their prey in the Wezmeh Cave (Kermanshah, Iran): A Late
524 Pleistocene refuge in the Zagros. International Journal of Osteoarchaeology 19, 678-694.
525 Maureille, B., Rougier, H., Houët, F., Vandermeersch, B., 2001. Les dents inférieures du
526 néandertalien Regourdou 1 (site de Regourdou, commune de Montignac, Dordogne): analyses
527 métriques et comparatives. Paléo 13, 183-200.
528 Mazurier, A., Bondioli, L., Caropreso, S., Macchiarelli, R., 2003. Topographic variation of the
529 enamel thickness in the human anterior deciduous dentition. American Journal of Physical
530 Anthropology 120(S36), 148.
531 Mitteroecker, P., Bookstein, F.L., 2011. Linear discrimination, ordination, and the visualization of
532 selection gradients in modern morphometrics. Evolutionary Biology 38, 100-114.
533 Mitteroecker, P., Gunz, P., Windhager, S., Schaefer, K., 2013. A brief review of shape, form, and
534 allometry in geometric morphometrics, with applications to human facial morphology. Hystrix
535 24, 59-66.
536 Moorrees, C.F.A., Fanning, E.A., Hunt, E.E., 1963. Age variation of formation stages for ten
537 permanent teeth. Journal of Dental Research 42, 1490-1502.
538 NESPOS Database, 2019. NEanderthal Studies Professional Online Service.
539 http://www.nespos.org.
540 Olejniczak, A.J., Smith, T.M., Feeney, R.N.M., Macchiarelli, R., Mazurier, A., Bondioli, L., Rosas,
541 A., Fortea, J., de la Rasilla, M., Garcia-Tabernero, A., Radovčić, J., Skinner, M.M., Toussaint,
542 M., Hublin, J.-J., 2008. Dental tissue proportions and enamel thickness in Neandertal and
543 modern human molars. Journal of Human Evolution 55, 12-23.
544 Otte, M., Biglari, F., Jaubert, J., Eds, 2009. Iran Palaeolithic. Archaeopress, Oxford.

Pan, L., Thackeray, J.F., Dumoncel, J., Zanolli, C., Oettlé, A., De Beer, F., Braga, J., 2017. Intra-individual metameric variation expressed at the enamel-dentine junction of lower post-canine dentition of South African fossil hominins and modern humans. American Journal of Physical Anthropology 163, 806-815.

Pomeroy, E., Lahr, M.M., Crivellaro, F., Farr, L., Reynolds, T., Hunt, C.O., Barker, G., 2017. Newly discovered Neanderthal remains from Shanidar Cave, Iraqi Kurdistan, and their attribution to Shanidar 5. Journal of Human Evolution 111, 102-118.

R Core Team, 2018. R: A language and environment for statistical computing. R Foundation for Statistical Computing, Vienna. http://www.R-project.org/.

Rosenberg, M., 1985. Report on the 1978 sondage at Eshkaft-e Gavi. Iran 23, 51-62.

Rougier, H., 2003. Etude descriptive et comparative de Biache-Saint-Vaast 1 (Biache-Saint-Vaast, Pas-de-Calais, France). Ph.D. Dissertation, Université de Bordeaux.

Schlager, S., 2019. Morpho: Calculations and visualizations related to geometric morphometrics. R package version 2.6. http://cran.r-project.org/web/packages/Morpho/index.html.

Schwartz, G.T., 2000. Taxonomic and functional aspects of the patterning of enamel thickness distribution in extant large-bodied hominoids. American Journal of Physical Anthropology 111, 211-244.

Scolan, H., Santos, F., Tillier, A.-M., Maureille, B., Quintard, A., 2012. Des nouveaux vestiges néanderthaliens à Las Pélénos (Monsempron-Libos, Lot-et-Garonne, France). Bulletins et Mémoires de la Société d'Anthropologie de Paris 24, 69-95.

Scott, J.E., Marean, C.W., 2009. Paleolithic hominin remains from Eshkaft-e Gavi (southern Zagros Mountains, Iran): description, affinities, and evidence for butchery. Journal of Human Evolution 57, 248-259.

568 Shidrang, S., Biglari, F., Bordes, J.-G., Jaubert, J., 2016. Continuity and change in the Late
569 Pleistocene lithic industries of the Central Zagros: A typo-technological analysis of lithic
570 assemblages from Ghar-e Khar Cave, Bisotun, Iran. Archaeology, Ethnology & Anthropology
571 of Eurasia 44, 27-38.
572 Skinner, M.M., Alemseged, Z., Gaunitz, C., Hublin, J.J., 2015. Enamel thickness trends in Plio-
573 Pleistocene hominin mandibular molars. Journal of Human Evolution 85, 35-45.
574 Skinner, M.M., Wood, B.A., Boesch, C., Olejniczak, A.J., Rosas, A., Smith, T. Hublin, J.-J., 2008.
575 Dental trait expression at the enamel-dentine junction of lower molars in extant and fossil
576 hominoids. Journal of Human Evolution 54, 173-186.
577 Smith, B.H., 1984. Patterns of molar wear in hunter-gatherers and agriculturalists. American
578 Journal of Physical Anthropology 63, 39-56.
579 Smith, T.M., Olejniczak, A.J., Kupczik, K., Lazzari, V., de Vos, J., Kullmer, O., Schrenk, F.,
580 Hublin, J.-J., Jacob, T., Tafforeau, P., 2009. Taxonomic assessment of the Trinil molars using
581 nondestructive 3D structural and development analysis. PaleoAnthropology 2009, 117-129.
582 Smith, T.M., Olejniczak, A.J., Zermeno, J.P., Tafforeau, P., Skinner, M.M., Hoffmann, A.,
583 Radovčić, J., Toussaint, M., Kruszynski, R., Menter, C., Moggi-Cecchi, J., Glasmacher, U.A.,
584 Kullmer, O., Schrenk, F., Stringer, C., Hublin, J.-J., 2012. Variation in enamel thickness within
585 the genus *Homo*. Journal of Human Evolution 62, 395-411.
586 Solecki, R.S., 1963. Prehistory in Shanidar valley, Northern Iraq. Science 139, 179-193.
587 Spoor, C.F., Zonneveld, F.W., Macho, G.A., 1993. Linear measurements of cortical bone and
588 dental enamel by computed tomography: Applications and problems. American Journal of
589 Physical Anthropology 91, 469-484.

590 Toussaint, M., 2014. The dentition of the Scladina 1-4A juvenile Neandertal. In: Toussaint, M.,
591 Bonjean, D., (Eds), The Scladina 1-4A Juvenile Neandertal (Andenne, Belgium):
592 Palaeoanthropology and Context. Université de Liège, Andenne, pp. 233-306.
593 Trinkaus, E. 1983. The Shanidar Neandertals. Academic Press, New York.
594 Trinkaus, E., 2018. Pleistocene human remains from Iran. In: Biglari, F., Shidrang, S., Mashkour,
595 M. (Eds), The Pleistocene Archaeology of the Iranian Plateau, Iraq and the Caucasus. National
596 Museum of Iran, Tehran, pp. 53-63.
597 Trinkaus, E., Biglari, F. 2006. Middle Paleolithic human remains from Bisitun cave, Iran.
598 Paléorient 32(2), 105-111.
599 Trinkaus, E., Biglari, F., Mashkour, M., Monchot, H., Reyss, J.L., Rougier, H., Heydari, S., Abdi,
600 K., 2008. Late Pleistocene human remains from Wezmeh Cave, Western Iran. American Journal
601 of Physical Anthropology 135, 371-378.
602 Tsanova, T., 2013. The beginning of the Upper Paleolithic in the Iranian Zagros. A taphonomic
603 approach and techno-economic comparison of Early Baradostian assemblages from Warwasi
604 and Yafteh (Iran). Journal of Human Evolution 65, 39-64.
605 Weber, G.W., Fornai, C., Gopher, A., Barkai, R., Sarig, R., Hershkovitz, I., 2016. The Qesem Cave
606 hominin material (part 1): A morphometric analysis of the mandibular premolars and molar.
607 Quaternary International 398, 159-174.
608 Xing, S., Martinón-Torres, M., Bermúdez de Castro, J.M., 2018. The fossil teeth of the Peking
609 Man. Scientific Reports 8, 2066.
610 Zanolli, C., 2015. Molar crown inner structural organization in Javanese *Homo erectus*. American
611 Journal of Physical Anthropology 156, 148-157.
612 Zanolli, C., Bondioli, L., Coppa, A., Dean, M.C., Bayle, P., Candilio, F., Capuani, S., Dreossi, D.,
613 Fiore, I., Frayer, D.W., Libsekal, Y., Mancini, L., Rook, L., Medin Tekle, T., Tuniz, C.,

614 Macchiarelli, R., 2014. The late Early Pleistocene human dental remains from Uadi Aalad and
615 Mulhuli-Amo (Buia), Eritrean Danakil: Macromorphology and microstructure. Journal of
616 Human Evolution 74, 96-113.
617 Zanolli, C., Kullmer, O., Kelley, J., Bacon, A.-M., Demeter, F., Dumoncel, J., Fiorenza, L., Grine,
618 F.E., Hublin, J.-J., Tuan, N.A., Huong, N.T.M., Pan, L., Schillinger, B., Schrenk, F., Skinner,
619 M.M., Ji, X., Macchiarelli, R., 2019. Evidence for increased hominid diversity in the Early-
620 Middle Pleistocene of Indonesia. Nature Ecology & Evolution 3, 755-764.
621 Zanolli, C., Martinón-Torres, M., Bernardini, F., Boschian, G., Coppa, A., Dreossi, D., Mancini,
622 L., Martínez de Pinillos, M., Martín-Francés L., Bermúdez de Castro J.M., Tozzi C., Tuniz C.
623 & Macchiarelli R., 2018a. The Middle Pleistocene (MIS 12) human dental remains from
624 Fontana Ranuccio (Latium) and Visogliano (Friuli-Venezia Giulia), Italy. A comparative high
625 resolution endostructural assessment. PLoS One 13, e0189773.
626 Zanolli, C., Pan, L., Dumoncel, J., Kullmer, O., Kundrát, M., Liu, W. Macchiarelli, R., Mancini,
627 L., Schrenk, F., Tuniz, C., 2018b. Inner tooth morphology of *Homo erectus* from Zhoukoudian.
628 New evidence from an old collection housed at Uppsala University, Sweden. Journal of Human
629 Evolution 116, 1-13.
630

Figure captions

Figure 1. a) Map of Paleolithic sites having yielded human remains in the Zagros Mountains across Iraq and Iran. b) The enlarged Iranian area showing the location of Wezmeh Cave.

Figure 2. a) The Wezmeh cave (white arrow) at the western foothills of the Qazivand Mountain, Kermanshah region of Central Western Zagros. b) Entrance of the cave and original location of the Late Pleistocene skeletal remains redeposited at the front of the cave mouth. c) Plan of the Wezmeh Cave with the areas of excavation (after Abdi et al., 2002); the area of the clandestine excavation is indicated at the top (black arrow). d) The Wezmeh 1 maxillary premolar in mesial (M), distal (D), buccal (B), lingual (L) and occlusal views (after Trinkaus et al., 2008).

Figure 3. µCT-based 3D virtual rendering of Wezmeh 1 a) external morphology; b) the specimen imaged with the virtually removed enamel cap revealing the morphology of the coronal dentine. The correspondence between the outer enamel and the inner dentine morphology can be appreciated in occlusal view for (1) the elevation of the mesial marginal ridge attached to a low short crest running into the mesial fovea and (2) a cusp-like relief on the distal marginal ridge. The arrows show the segments of the bifurcated transverse crest and the asterisks indicate the position of small pits representing minor enamel defects.

Figure 4. Plot of log 2D average enamel thickness (2D AET) against log coronal dentine and pulp area (b) for Wezmeh 1 and the P^3 and P^4 forming the Neanderthal (NEA), Middle Paleolithic

modern human (MPMH), and Western European Holocene human (HH) samples. See Tables 1 and 2 and SOM Table S1 for sample composition.

Figure 5. Enamel thickness cartographies of Wezmeh 1 in occlusal (O), buccal (B), mesial (M), lingual (L), and distal (D) views compared with selected P^3 from the Neanderthal (NEA), Middle Paleolithic modern human (MPMH), and Western European Holocene human (HH) samples. Topographic thickness variation is rendered by a pseudocolor scale ranging from thinner dark blue to thicker red; isolated spots correspond to wear-related enamel removal. Independently from their original side, all crowns are shown as right.

Figure 6. Enamel thickness cartographies of Wezmeh 1 in occlusal (O), buccal (B), mesial (M), lingual (L), and distal (D) views compared with selected P^4 from the Neanderthal (NEA), Middle Paleolithic modern human (MPMH), and Western European Holocene human (HH) samples. Topographic thickness variation is rendered by a pseudocolor scale ranging from thinner dark blue to thicker red; isolated spots correspond to wear-related enamel removal. Independently from their original side, all crowns are shown as right.

Figure 7. Between-group principal component analysis (bgPCA) of the Procrustes shape coordinates of the enamel-dentine junction (EDJ) of Wezmeh 1 compared with the P^3 and P^4 forming the Neanderthal (NEA), Middle Paleolithic modern human (MPMH), and Western European Holocene human (HH) samples. See Tables 1 and 2 and SOM Table S1 for sample composition. The extremes of morphological variation are illustrated at the ends of each bgPC axis in occlusal (mesial aspect, upward) and buccal views (mesial aspect, rightward).

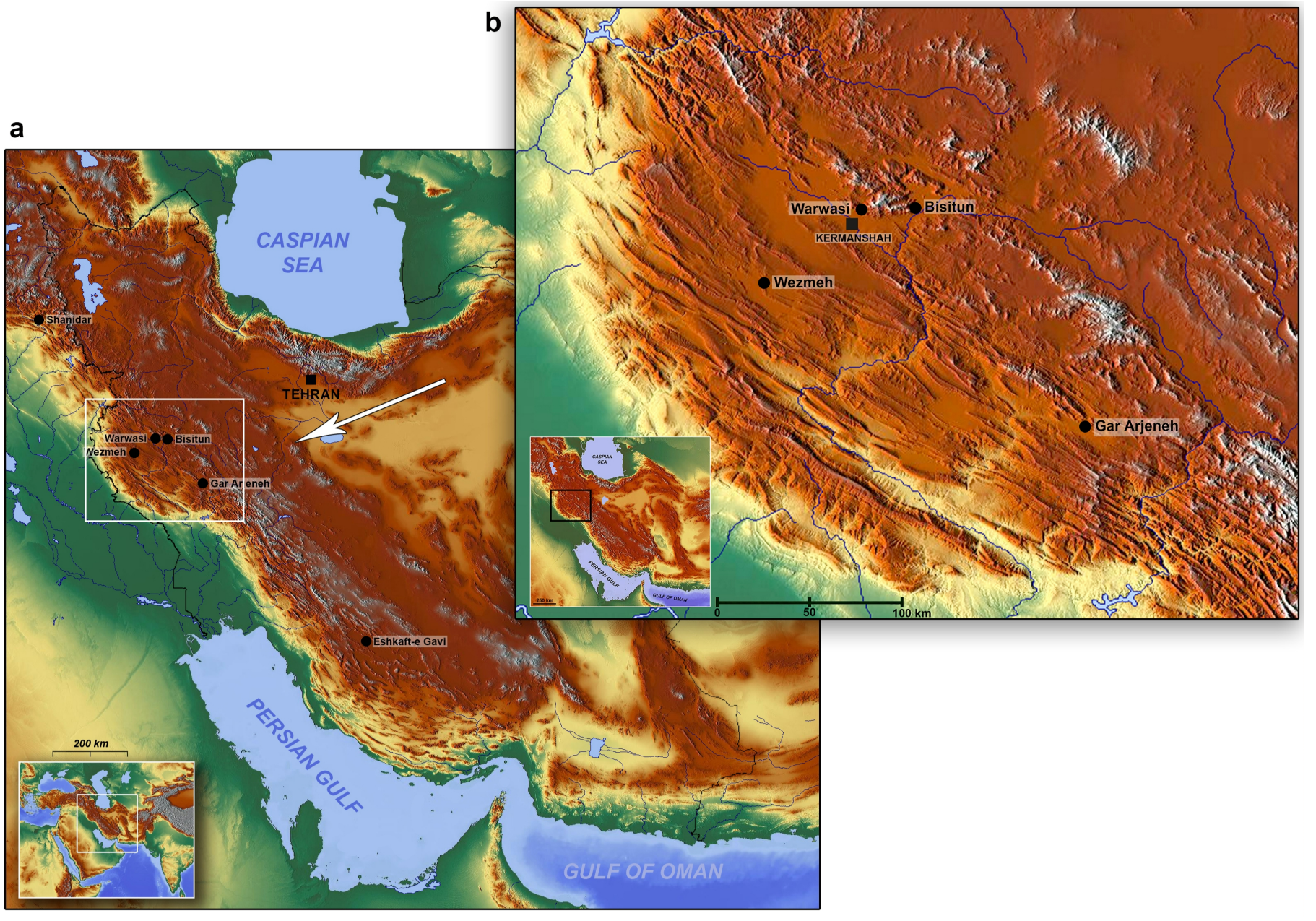
a
b
CASPIAN SEA
Shanidar
TEHRAN
Warwasi
Bisitun
Wezmeh
Gar Arjeneh
Eshkaft-e Gavi
PERSIAN GULF
GULF OF OMAN
200 km
KERMANSHAH
0
50
100 km

a

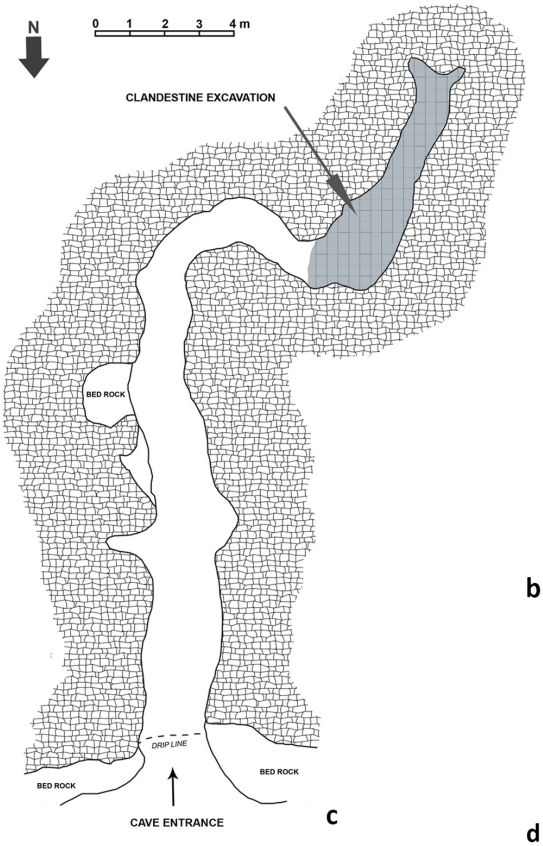
N
0 1 2 3 4 m
CLANDESTINE EXCAVATION
BED ROCK
DRIP LINE
BED ROCK
BED ROCK
CAVE ENTRANCE

c

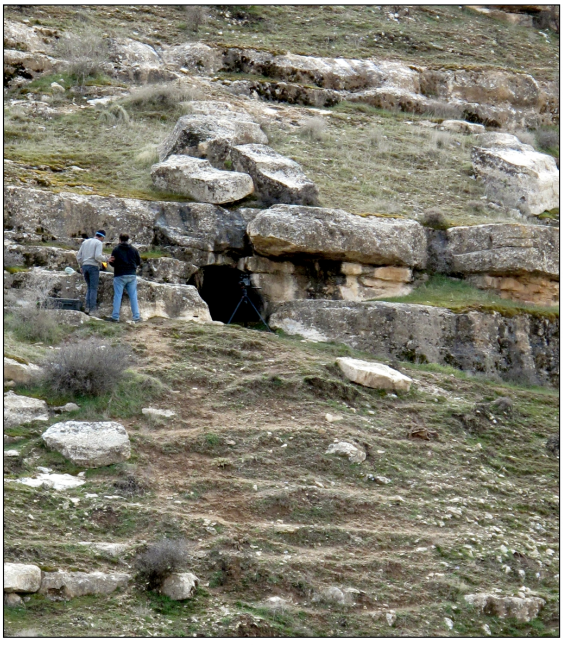

b


M
D
B
L

d

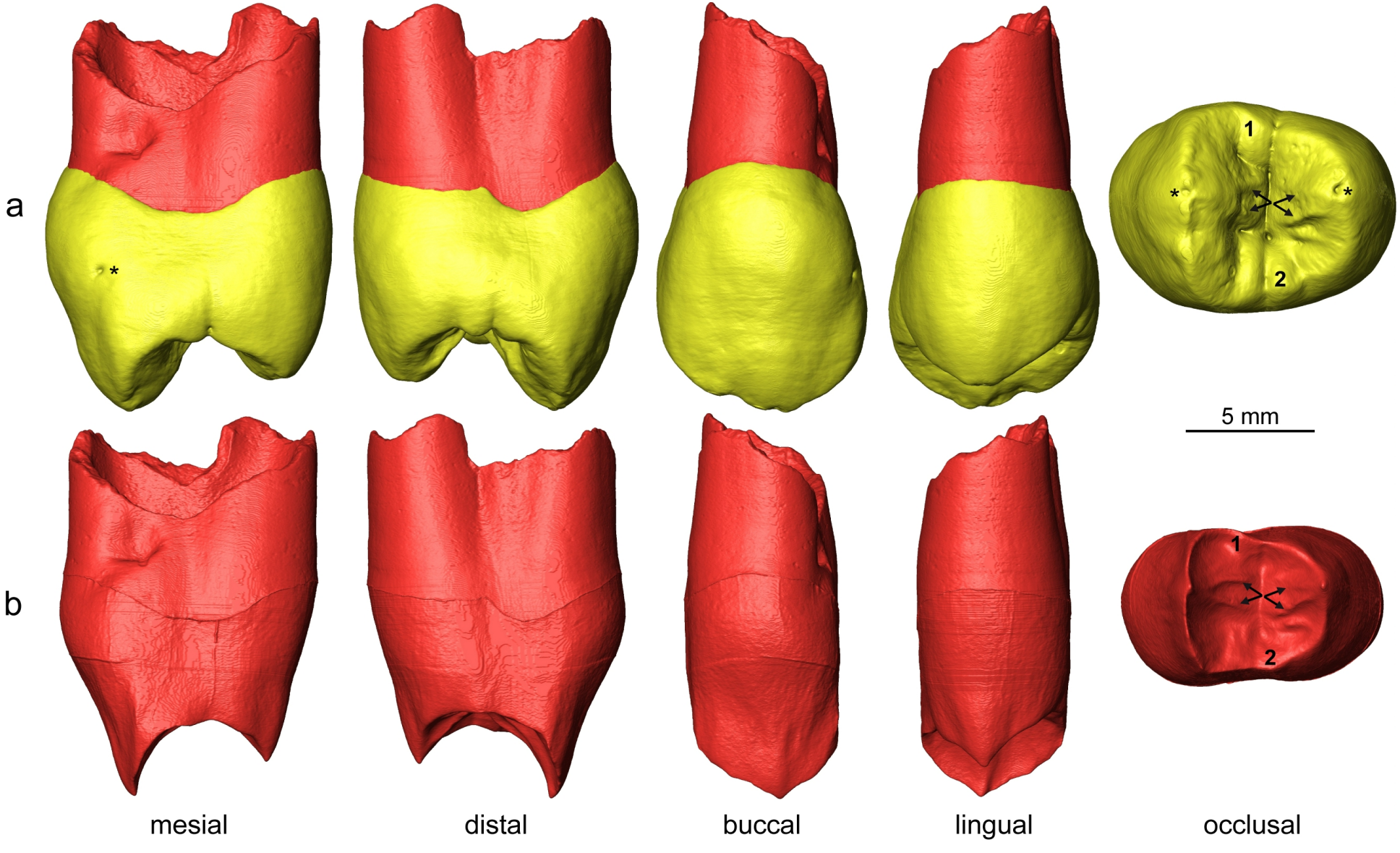
a
b
*
*
*
1
2
1
2
5 mm
mesial
distal
buccal
lingual
occlusal

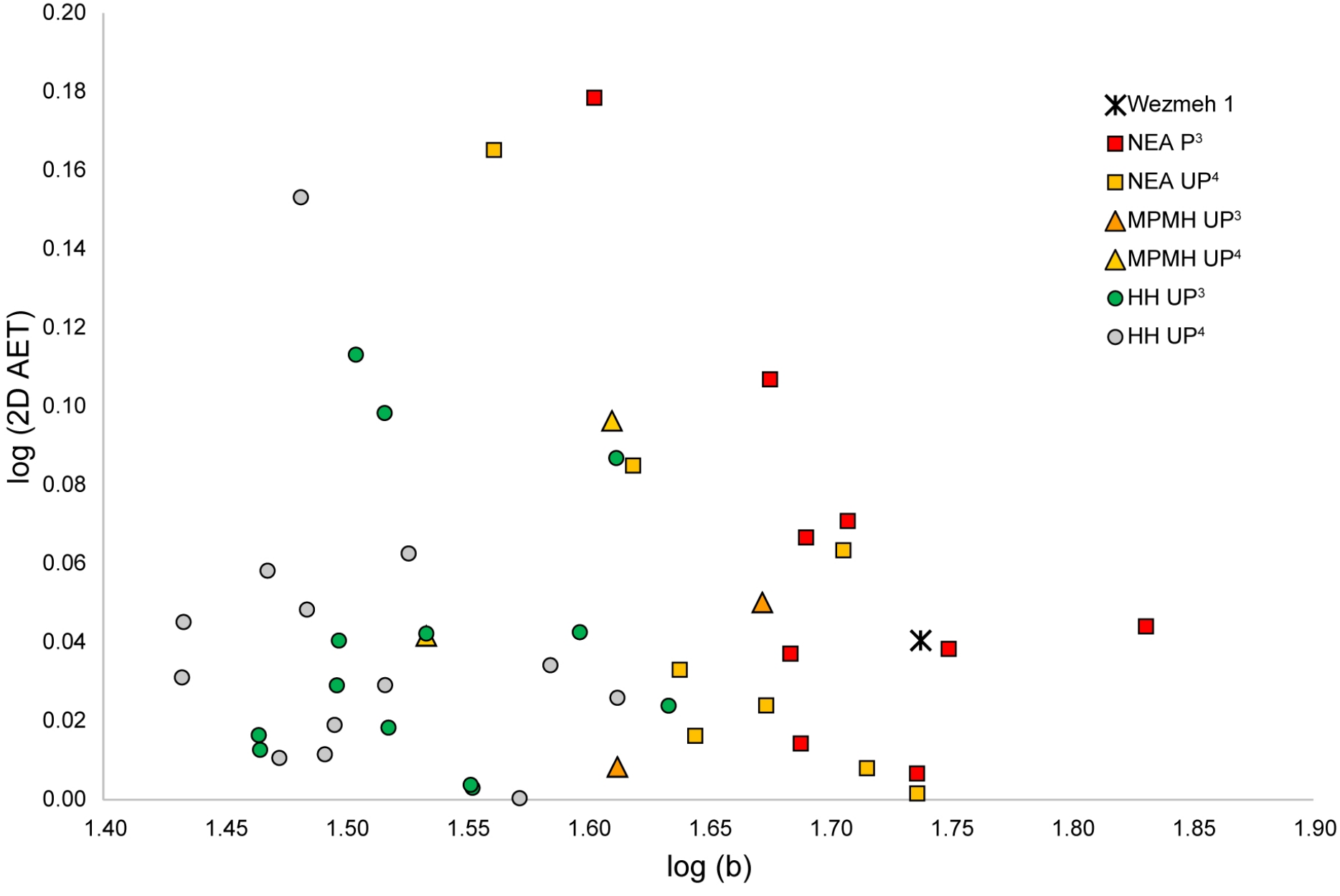
0.20
0.18
0.16
0.14
0.12
0.10
0.08
0.06
0.04
0.02
0.00
log (2D AET)
1.40
1.45
1.50
1.55
1.60
1.65
1.70
1.75
1.80
1.85
1.90
log (b)
Wezmeh 1
NEA P3
NEA UP4
MPMH UP3
MPMH UP4
HH UP3
HH UP4

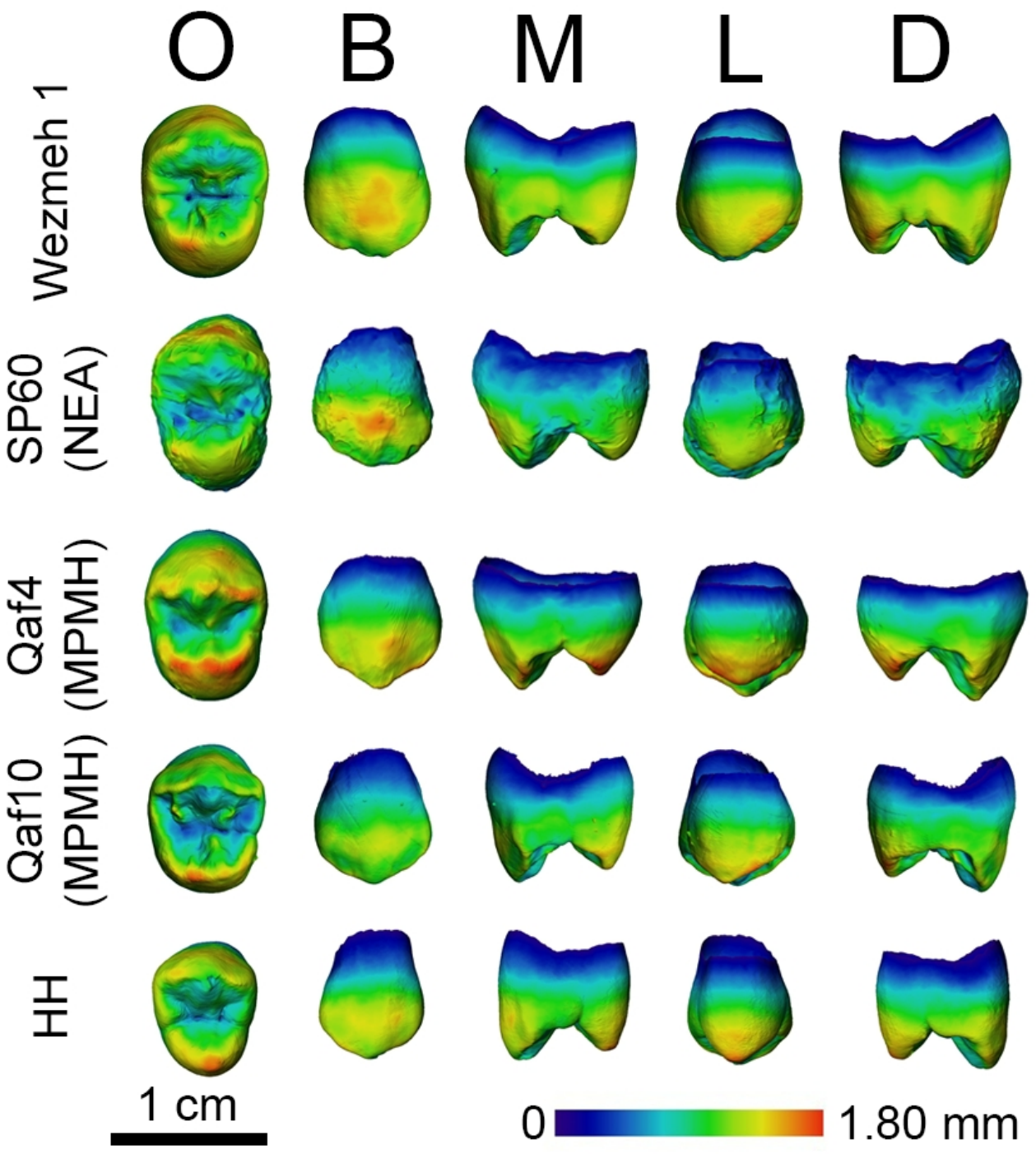
O
B
M
L
D
Wezmeh 1
SP60 (NEA)
Qaf4 (MPMH)
Qaf10 (MPMH)
HH
1 cm
0
1.80 mm

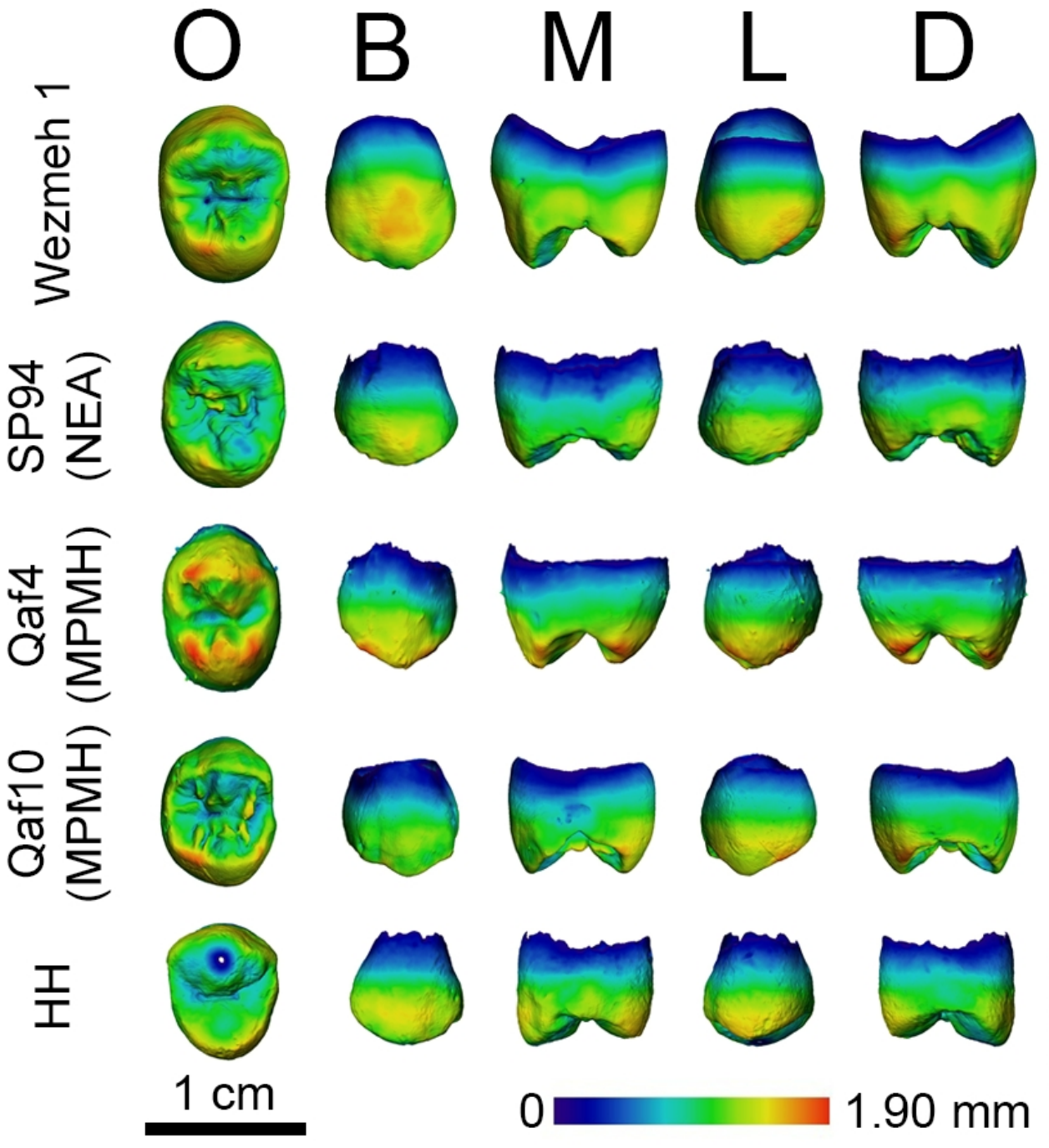
O
B
M
L
D
Wezmeh 1
SP94 (NEA)
Qaf4 (MPMH)
Qaf10 (MPMH)
HH
1 cm
0
1.90 mm

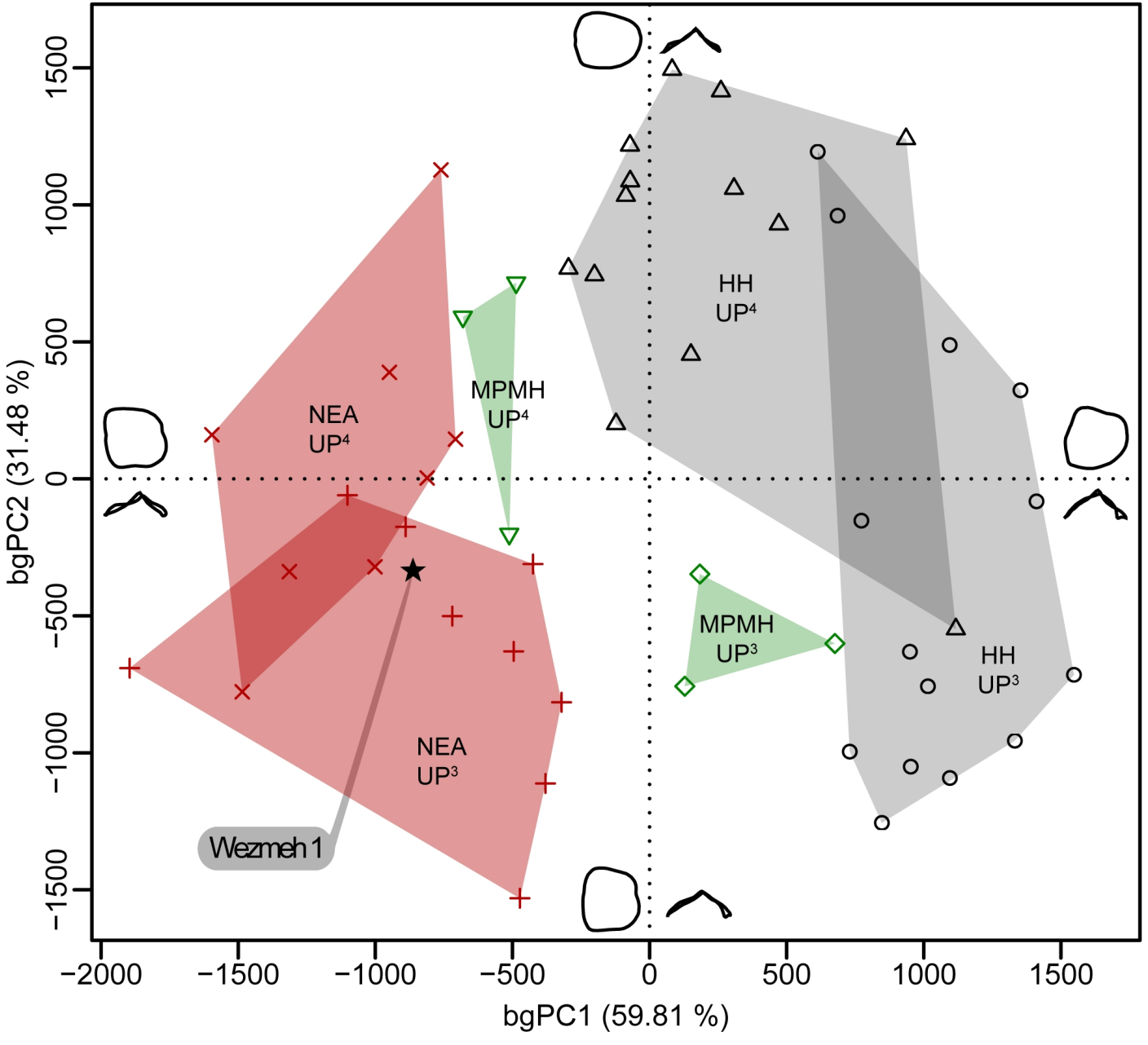
NEA
UP4
MPMH
UP4
HH
UP4
MPMH
UP3
HH
UP3
NEA
UP3
Wezmeh 1
bgPC1 (59.81 %)
bgPC2 (31.48 %)
−2000
−1500
−1000
−500
0
500
1000
1500
−1500
−1000
−500
0
500
1000
1500

Table 1

Number of specimens (*n*) and degree of occlusal wear (range; Smith, 1984) of the P^3 and P^4 forming the three comparative samples used in the 2-3D analyses. The samples represent Neanderthals (NEA), Middle Paleolithic modern humans (MPMH) and Western European Holocene humans (HH).

Tooth	Sample	*n*	Wear degree	*n* GM EDJ	*n* DTP and ET 2D	*n* DTP and ET 3D (wear degree ≤ 2)	*n* TOPO ET 2D	2-3D data sources
P^3	NEA	9	1–4	9	9	4	9	Bayle et al., 2017, 2019; NESPOS Database, 2019
	MPMH	3	1	3	2	2	3	ESRF Paleontological Microtomographic Database, 2019; original data
	HH	14	1–4	14	13	11	13	Le Luyer, 2016; original data
P^4	NEA	8	1–4	8	8	4	8	Bayle et al., 2017, 2019; NESPOS Database, 2019

MPMH	3	1	3	2	2	3	ESRF Paleontological Microtomographic Database, 2019; original data
HH	13	1–4	13	13	11	13	Le Luyer, 2016; original data

Abbreviations: GM EDJ = geometric morphometrics of the enamel-dentine junction shape; DTP dental tissue proportions; ET = enamel thickness; TOPO ET: standardized enamel thickness topographic variation.

Table 2

List of the P^3 and P^4 forming the Neanderthal (NEA) and the Middle Paleolithic modern human (MPMH) samples used in the comparative analyses. See Table 1 for the data sources.

	P^3	P^4
NEA	KRD38, KRD39, KRD43, KRD45, KRD48, Palomas 53, Palomas 60, Palomas 68, Spy11F	KRD41, KRD42, KRD44, KRD46, KRD47, Palomas 68, Palomas 94, Spy 11E
MPMH	Qafzeh 4, Qafzeh 10, Qafzeh 15	Qafzeh 4, Qafzeh 10, Qafzeh 15

Table 3

2D dental tissue proportions and enamel thickness in Wezmeh 1 compared to the values of the P^3 and P^4 forming the Neanderthal (NEA), Middle Paleolithic modern human (MPMH), and Western European Holocene human (HH) samples. See Tables 1 and 2 for sample composition.

		c (mm^2)	b (mm^2)	a (mm^2)	b/a	e (mm)	BCD (mm)	2D AET (mm)	2D RET
Wezmeh 1		27.16	54.72	81.88	66.83	24.75	9.86	1.10	14.83
NEA P^3	mean	22.21	51.44	73.66	69.98	22.78	9.83	0.97	13.59
	range	13.73–26.93	40.08–67.76	53.81–91.60	65.25–74.48	20.71–26.39	8.52–10.94	0.66–1.18	10.47–16.65
NEA P^4	mean	21.50	46.26	67.76	68.37	21.47	9.75	1.00	14.70
	range	13.37–25.42	36.43–54.49	49.80–76.56	62.06–73.15	19.56–22.52	8.04–11.44	0.68–1.22	11.32–18.86
MPMH P^3	mean	22.34	44.00	66.34	66.29	20.86	8.90	1.07	16.15
	range	21.33–23.35	40.97–47.03	62.30–70.38	65.76–66.82	20.80–20.92	7.74–10.05	1.02–1.12	15.93–16.37
MPMH P^4	mean	23.43	37.46	60.89	61.51	19.93	8.81	1.18	19.20
	range	21.63–25.22	34.16–40.76	55.79–65.98	61.23–61.78	19.65–20.20	7.99–9.63	1.10–1.25	18.83–19.56
HH P^3	mean	18.62	34.44	53.06	64.85	19.48	7.61	0.96	16.43
	range	14.31–21.55	29.12–43.02	45.66–64.17	59.44–70.34	17.18–22.35	6.84–8.42	0.77–1.10	12.80–19.58
HH P^4	mean	19.99	32.27	52.26	61.72	18.88	7.87	1.06	18.79
	range	15.27–26.81	27.07–40.97	45.43–62.99	53.06–66.63	17.07–21.94	7.08–8.60	0.89–1.42	14.91–25.85

Abbreviations: 2D AET = 2D average enamel thickness; 2D RET = 2D relative enamel thickness; a = total crown area; b =: coronal dentine and pulp area; b/a = percentage of crown area that is dentine and pulp; c = enamel area; e = enamel-dentine junction length; BCD = bicervical diameter.

Table 4

3D dental tissue proportions and enamel thickness in Wezmeh 1 compared to the values of the P^3 and P^4 forming the Neanderthal (NEA), Middle Paleolithic modern human (MPMH), and Western European Holocene human (HH) samples. See Tables 1 and 2 for sample composition.

		Ve (mm^3)	Vcdp (mm^3)	Vc (mm^3)	Vcdp/Vc	SEDJ (mm^2)	3D AET (mm)	3D RET
Wezmeh 1		204.48	208.89	413.37	50.53	177.27	1.15	19.44
NEA P^3	mean	141.04	165.28	306.32	54.66	145.07	0.95	17.27
	range	85.15–202.97	111.97–199.26	197.12–402.23	49.54–57.72	112.80–168.28	0.75–1.23	15.64–21.02
NEA P^4	mean	143.72	166.92	310.64	53.56	137.92	1.02	18.76
	range	83.94–179.04	96.16–221.02	180.10–383.33	51.39–57.66	102.55–154.54	0.82–1.18	17.37–20.40
MPMH P^3	mean	147.15	153.11	300.25	51.00	136.38	1.08	20.14
	range	134.91–159.38	140.58–165.63	275.49–325.00	50.96–51.03	132.01–140.75	1.02–1.13	19.65–20.62
MPMH P^4	mean	141.15	131.50	272.64	48.19	119.05	1.19	23.31
	range	132.42–149.87	120.11–142.88	252.53–292.75	47.56–48.81	115.80–122.29	1.14–1.23	23.18–23.44
HH P^3	mean	115.04	111.73	226.76	49.27	113.86	1.02	21.23
	range	80.93–141.78	88.37–144.50	186.93–282.73	41.00–56.70	98.68–135.26	0.75–1.29	15.81–28.93
HH P^4	mean	117.22	102.65	219.86	46.61	107.41	1.09	23.51
	range	88.65–152.91	80.88–134.07	181.95–281.97	41.84–53.68	93.19–126.66	0.85–1.29	17.85–27.89

Abbreviations: 3D AET = 3D average enamel thickness; 3D RET = 3D relative enamel thickness; SEDJ = EDJ surface area; Vc = total crown volume; Vcdp = coronal dentine and pulp volume; Vcdp/Vc = percentage of crown volume that is dentine and pulp; Ve = enamel volume.

Supplementary Online Material (SOM):

A Neanderthal from the Central Western Zagros, Iran. Structural reassessment of the Wezmeh 1 maxillary premolar

Clément Zanolli [a, *], Fereidoun Biglari [b, *], Marjan Mashkour [c, d], Kamyar Abdi [e], Hervé Monchot [f], Karyne Debue [c], Arnaud Mazurier [g], Priscilla Bayle [a], Mona Le Luyer [a, h], Hélène Rougier [i], Erik Trinkaus [j], Roberto Macchiarelli [k,l]

[a] *Laboratoire PACEA, UMR 5199 CNRS, Université de Bordeaux, Ministère de la Culture, Bordeaux, France*

[b] *Paleolithic Department, National Museum of Iran, Tehran, Iran*

[c] *Laboratoire AASPH, UMR 7209 CNRS, Muséum national d'Histoire naturelle, Paris, France*

[d] *Archaeozoology Section, Bioarchaeology Laboratory, Central Laboratory, University of Tehran, Tehran, Iran*

[e] *University of Shiraz, Shiraz, Iran*

[f] *UMR 8167 Orient et Méditerranée, Paris Sorbonne Universités, Paris, France*

[g] *Institut de Chimie des Milieux et Matériaux, UMR 7285 CNRS, Université de Poitiers, Poitiers, France*

[h] *Skeletal Biology Research Centre, School of Anthropology and Conservation, University of Kent, Canterbury, UK*

[i] *Department of Anthropology, California State University, Northridge, CA 91330, USA*

[j] *Department of Anthropology, Washington University, Saint Louis, MO 63130, USA*

[k] *Laboratoire HNHP, UMR 7194 CNRS, Muséum national d'Histoire naturelle, Musée de l'Homme, Paris, France*

[l] *Unité de Formation Géosciences, Université de Poitiers, Poitiers, France*

* Corresponding authors.

E-mail addresses: clement.zanolli@gmail.com (C. Zanolli), fbiglari@gmail.com (F. Biglari).

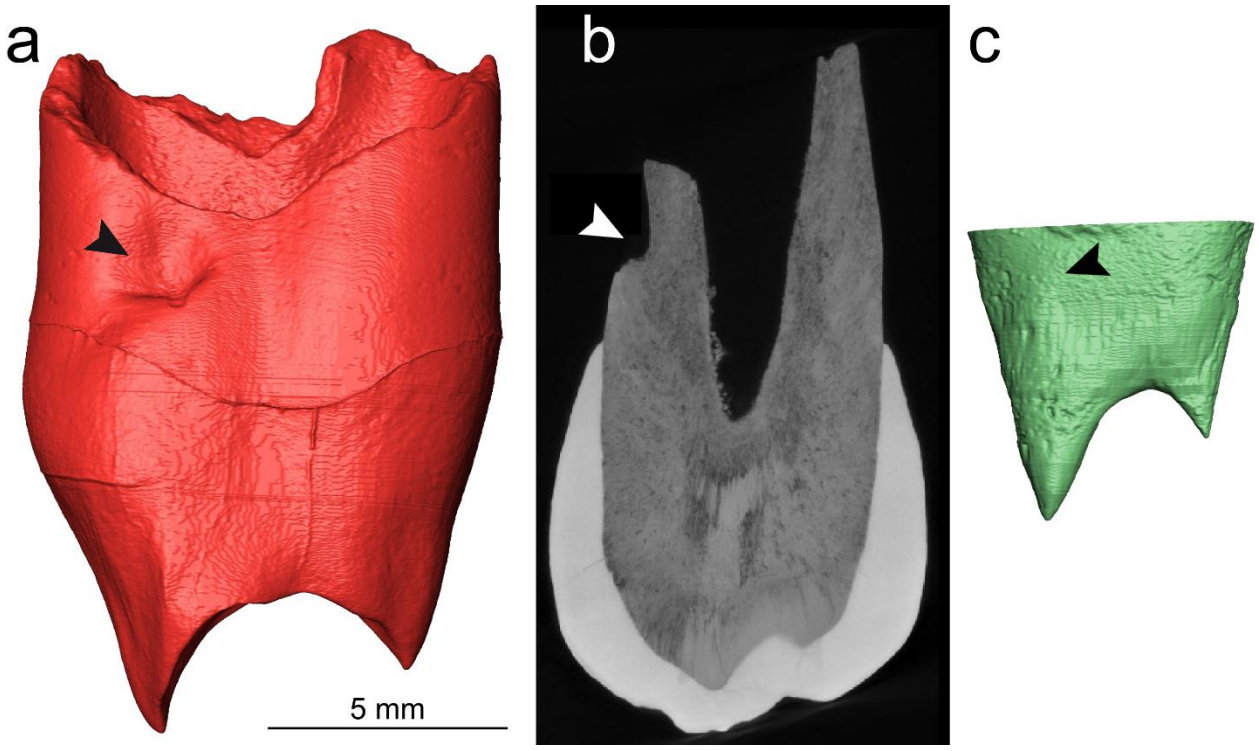

SOM Figure S1. a) µCT-based 3D virtual rendering of the Wezmeh 1 coronal and radicular dentine in mesial view showing the relatively large and deep depression on the root, approximately 2.0 mm from the cervix (arrow). b) Virtual section across the depression (arrow) revealing that it does not reach the inner dentine wall (dentine-pulp junction). c) As visible on the section, this defect does not affect the still forming pulp chamber.

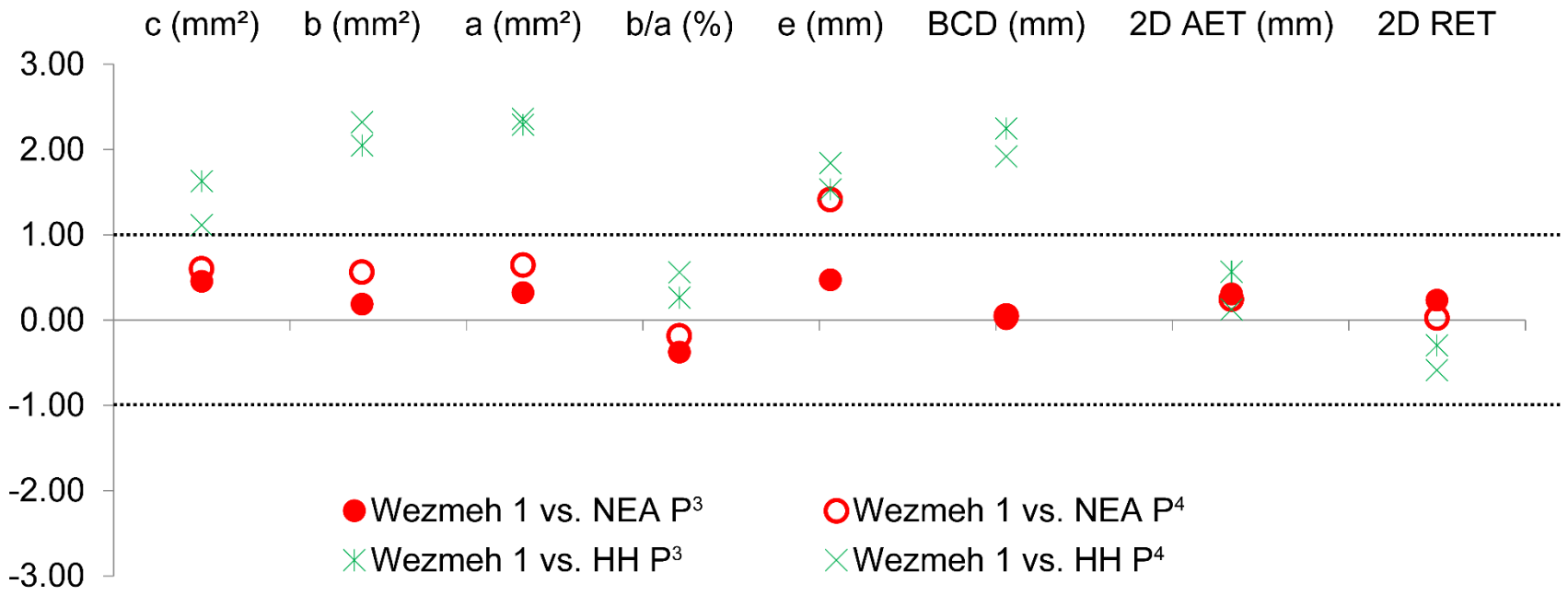

SOM Figure S2. Adjusted Z-scores of the 2D dental tissue proportions and enamel thickness variables in Wezmeh 1 compared to the variation expressed by the P^3 and P^4 premolars forming the Neanderthal (NEA), Middle Paleolithic modern human (MPMH), and Western European Holocene human (HH) samples. The line passing through zero represents the mean; the dotted lines correspond to the estimated 95% limit of variation expressed by the comparative samples. See Materials and methods for variable abbreviations and Tables 1 and 2 and SOM Table S1 for sample composition.

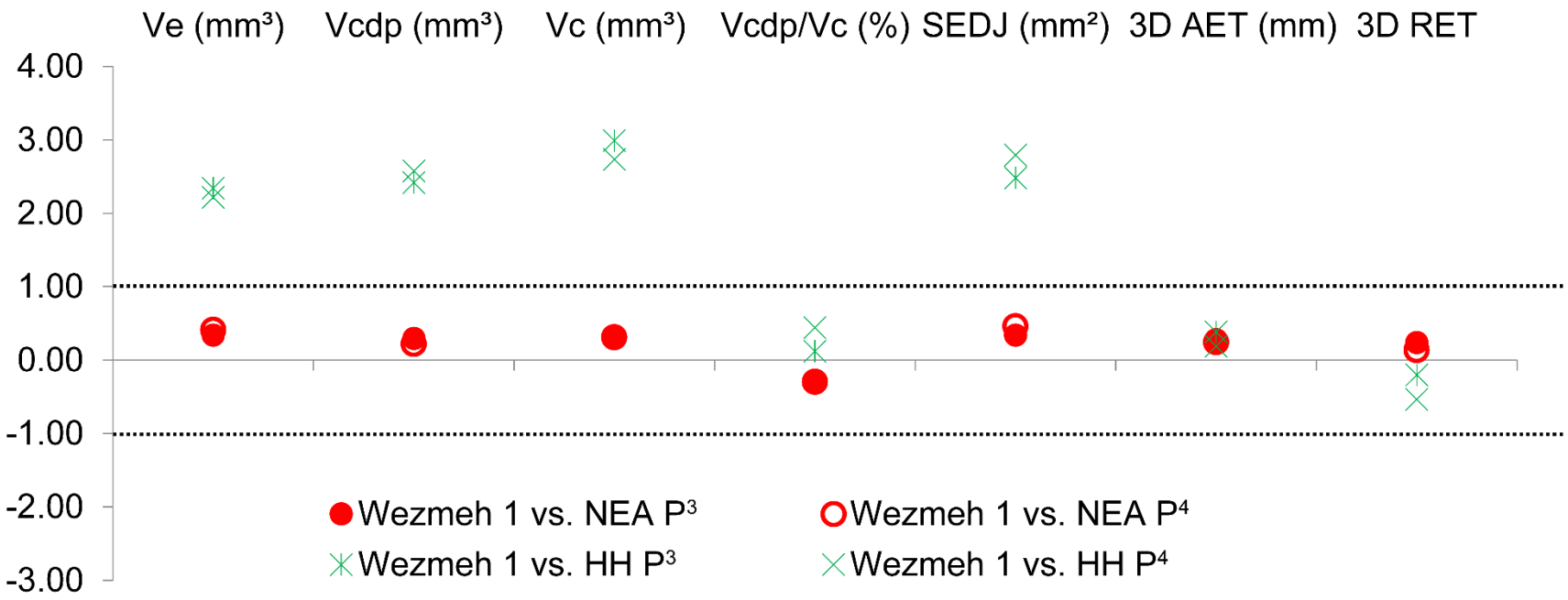

SOM Figure S3. Adjusted Z-scores of the 3D dental tissue proportions and enamel thickness variables in Wezmeh 1 compared to the variation expressed by the P^3 and P^4 forming the Neanderthal (NEA), Middle Paleolithic modern human (MPMH), and Western European Holocene human (HH) samples. The line passing through zero represents the mean; the dotted lines correspond to the estimated 95% limit of variation expressed by the comparative samples. See Materials and methods for variable abbreviations and Tables 1 and 2 and SOM Table S1 for sample composition.

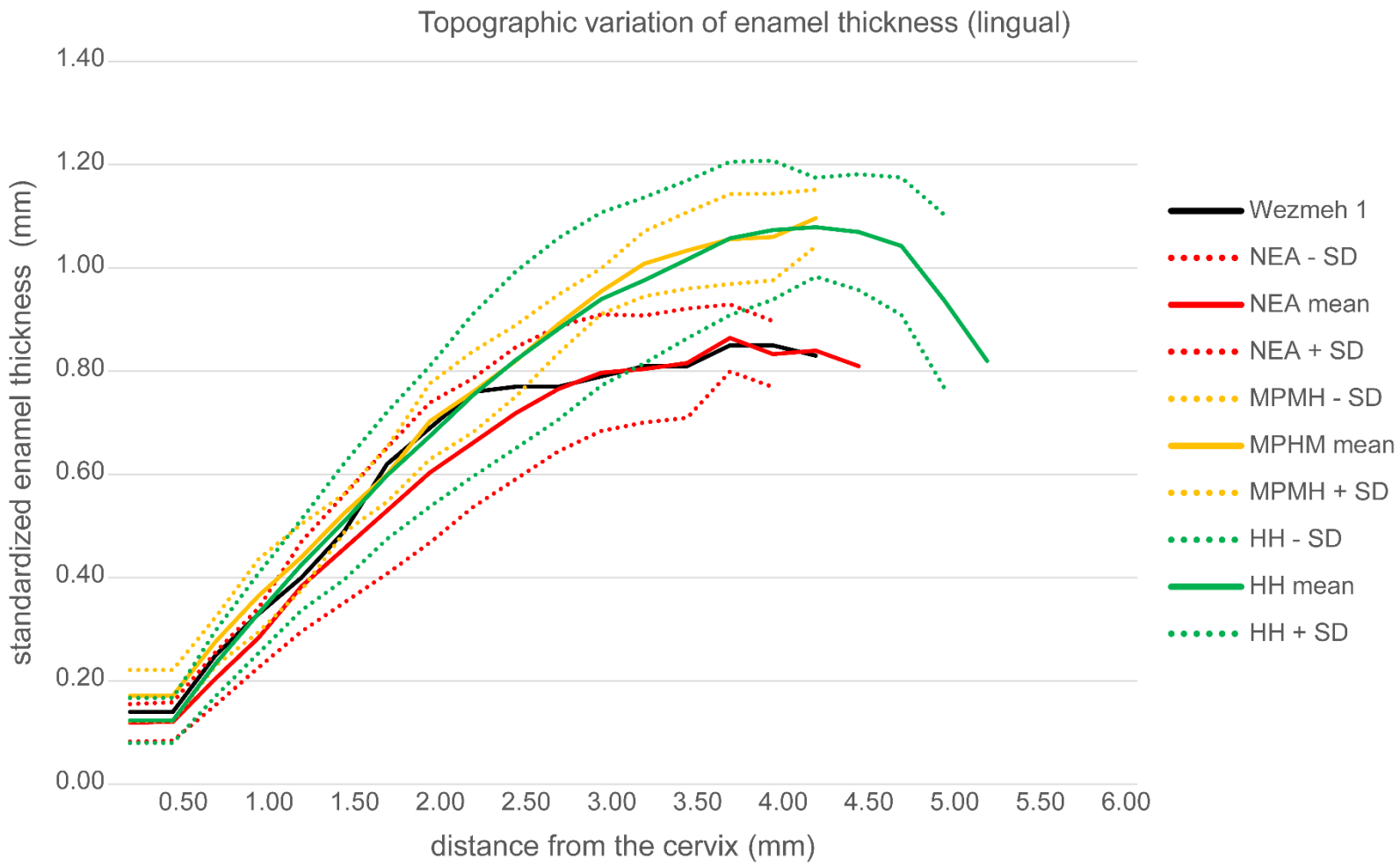

SOM Figure S4. Standardized enamel thickness topographic variation (in mm) measured across the entire virtual lingual section in Wezmeh 1 compared with the values measured on the homologous virtual sections of the pooled P^3 and P^4 forming the Neanderthal (NEA; mean ± 1 SD), Middle Paleolithic modern human (MPMH; mean ± 1 SD), and Western European Holocene human (HH; mean ± 1 SD) samples.

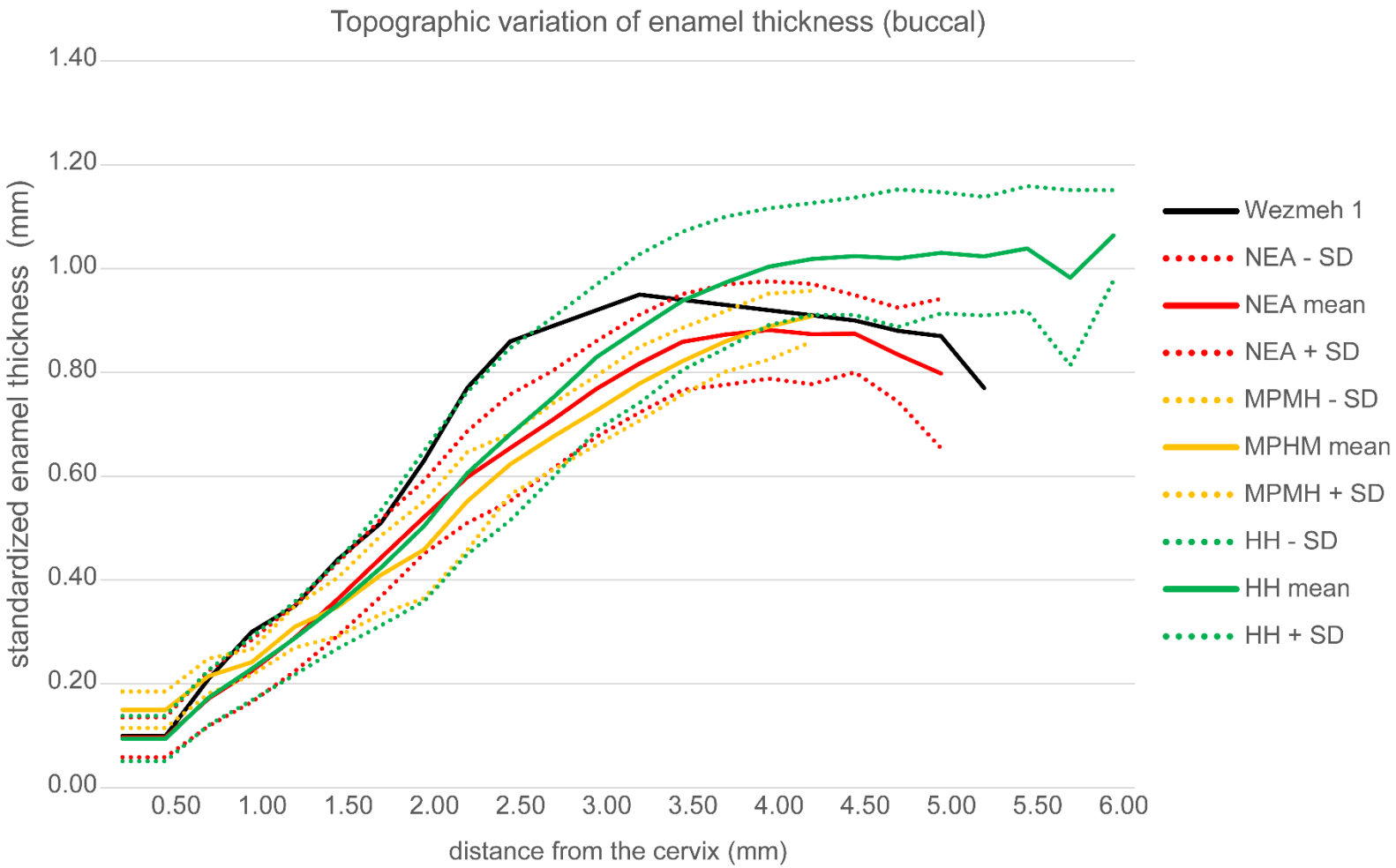

SOM Figure S5. Standardized enamel thickness topographic variation (in mm) measured across the entire virtual buccal section in Wezmeh 1 compared with the values measured on the homologous virtual sections of the pooled P^3 and P^4 forming the Neanderthal (NEA; mean ± 1 SD), Middle Paleolithic modern human (MPMH; mean ± 1 SD), and Western European Holocene human (HH; mean ± 1 SD) samples.

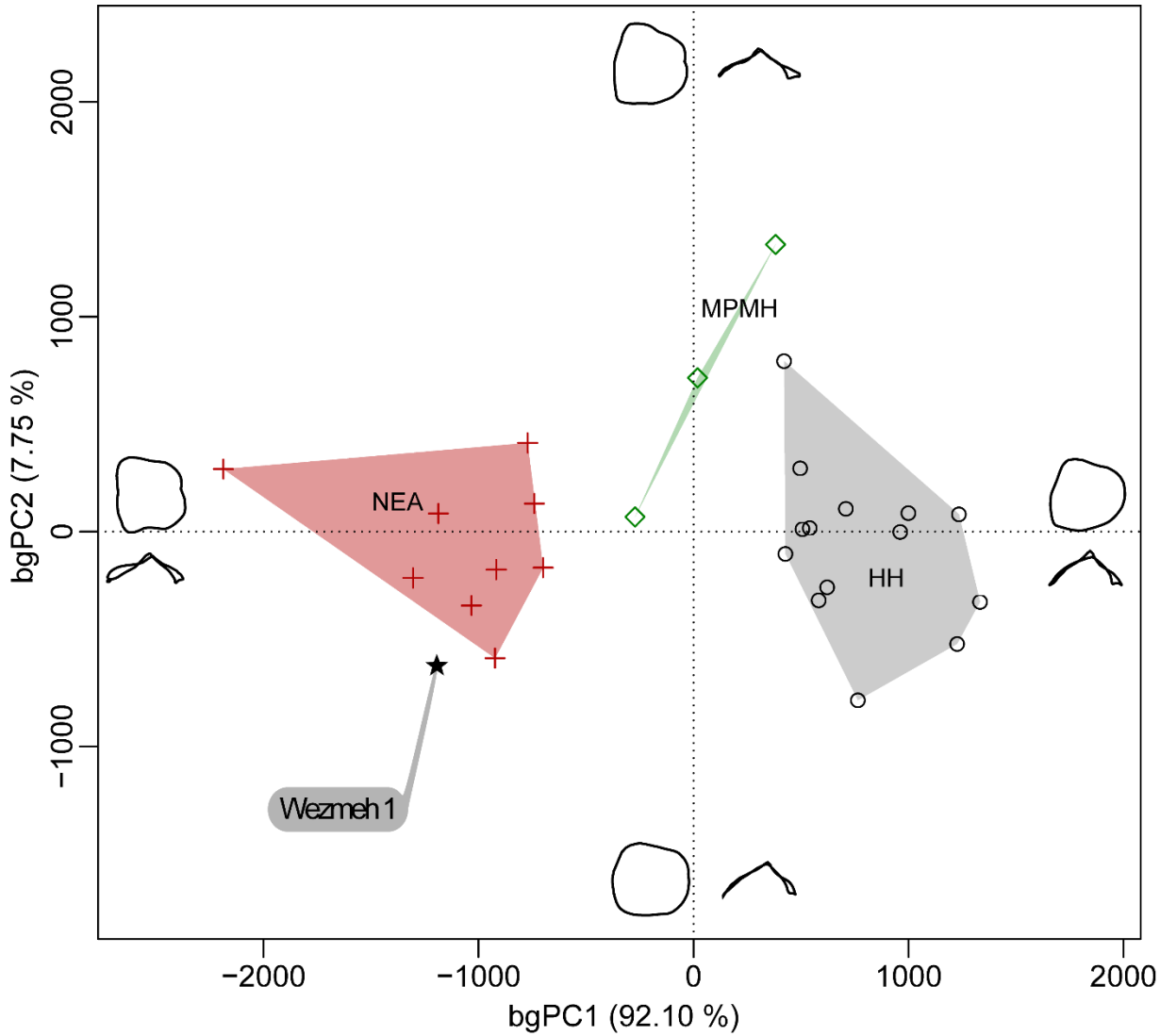
2000
1000
0
−1000
bgPC2 (7.75 %)
−2000
−1000
0
1000
2000
bgPC1 (92.10 %)
NEA
MPMH
HH
Wezmeh1

SOM Figure S6. Between-group principal component analysis (bgPCA) of the Procrustes shape coordinates of the enamel-dentine junction (EDJ) of Wezmeh 1 compared with the P^3 forming the Neanderthal (NEA), Middle Paleolithic modern human (MPMH), and Western European Holocene human (HH) samples.

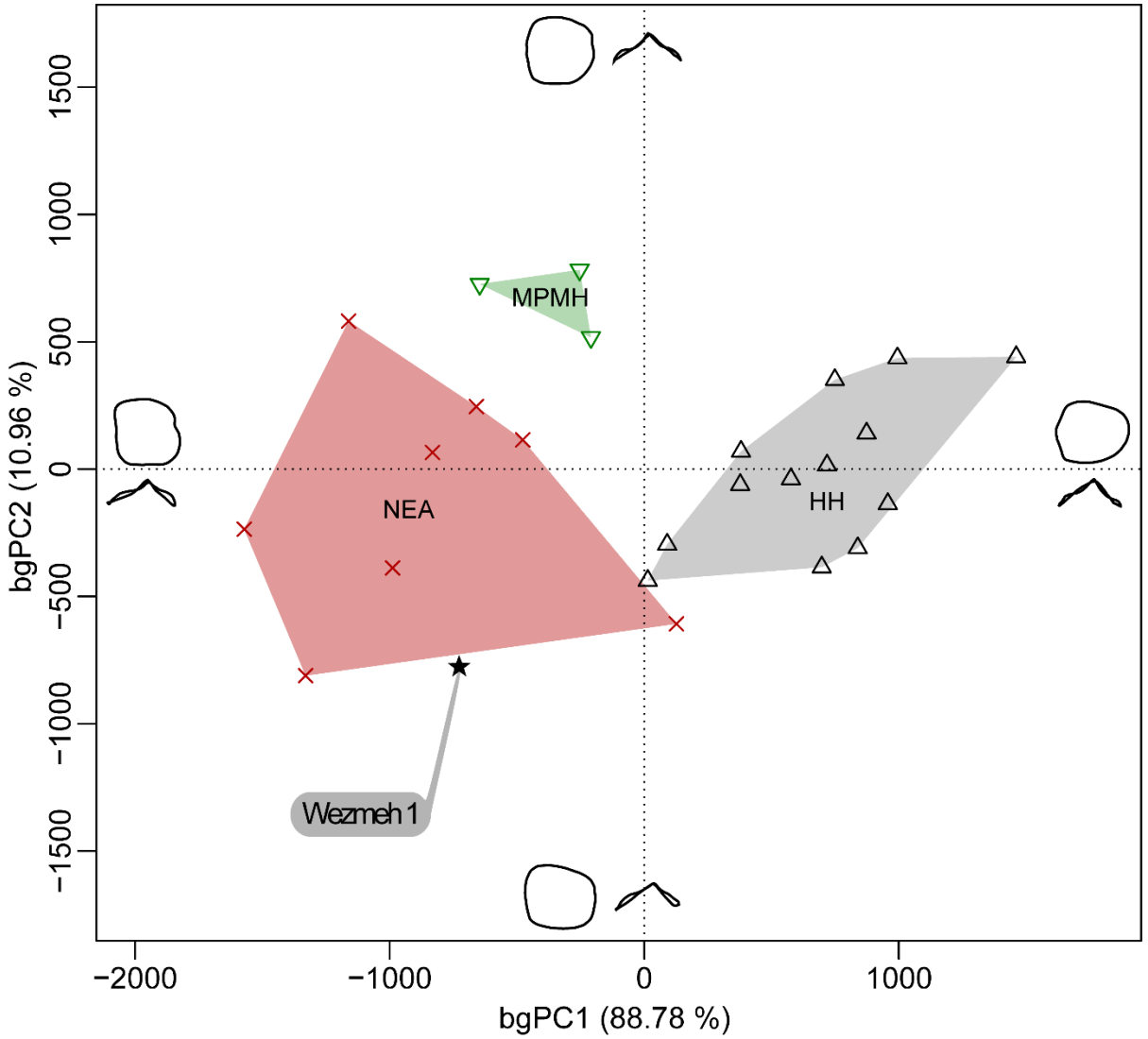
MPMH
NEA
HH
Wezmeh1
bgPC1 (88.78 %)
bgPC2 (10.96 %)
−2000
−1000
0
1000
1500
1000
500
0
−500
−1000
−1500

SOM Figure S7. Between-group principal component analysis (bgPCA) of the Procrustes shape coordinates of the enamel-dentine junction (EDJ) of Wezmeh 1 compared with the P^4 forming the Neanderthal (NEA), Middle Paleolithic modern human (MPMH), and Western European Holocene human (HH) samples.

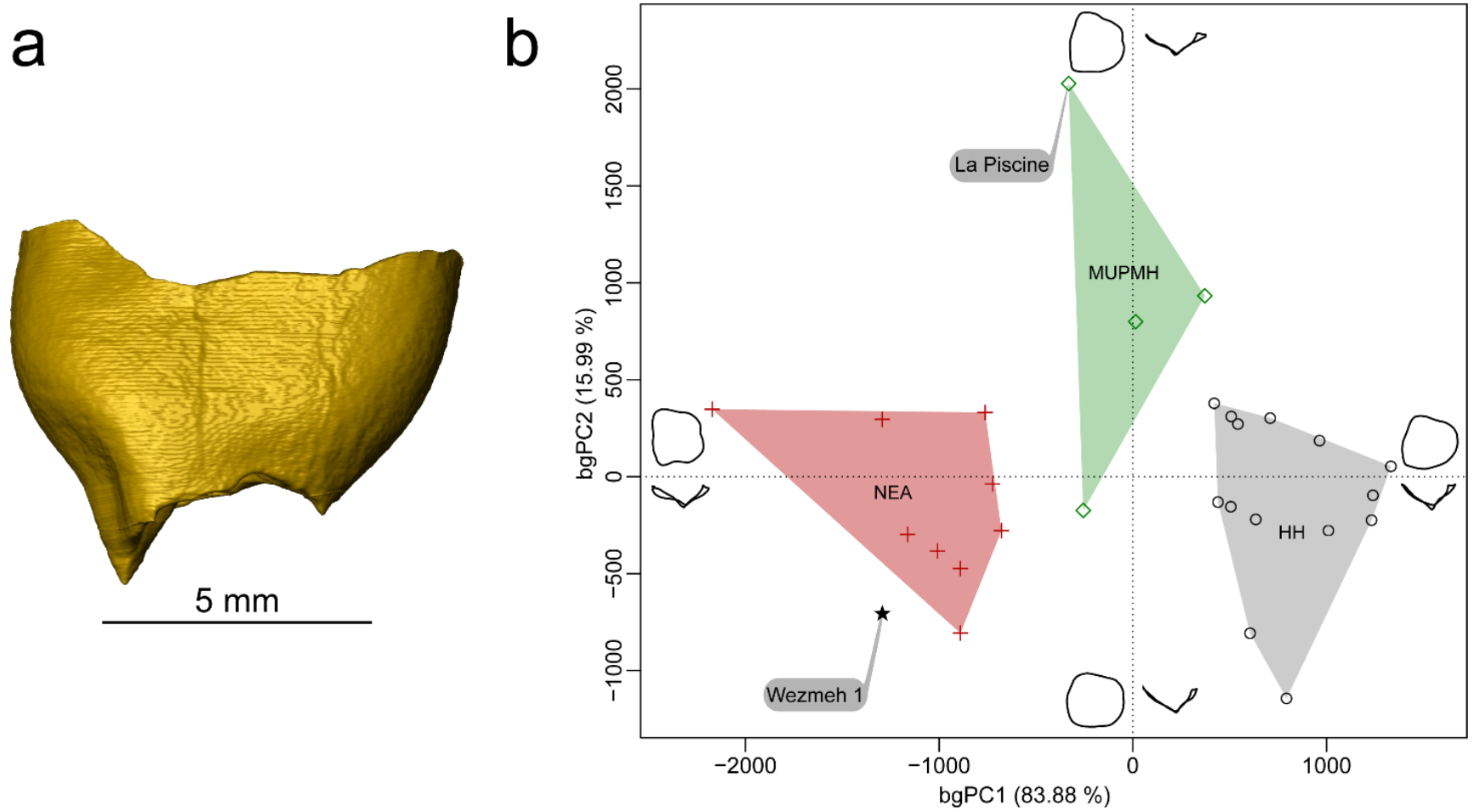

SOM Figure S8. a) Virtual rendering of the EDJ of the late Upper Paleolithic (Magdalenian) P^3 H3 from the French site of La Piscine. Stored at the Musée d'Art et d'Histoire de Montmorillon (http://sitearcheo-la-piscine.blogspot.com), H3 was µCT-scanned in 2010 at the University of Poitiers (voxel size of 14.46 µm) thanks to the scientific collaboration provided by C. Delage. b) Between-group principal component analysis (bgPCA) of the Procrustes shape coordinates of the enamel-dentine junction (EDJ) of H3 compared with Wezmeh

1 and the P^3 forming the Neanderthal (NEA), Middle Paleolithic modern human (MPMH), and Western European Holocene human (HH) samples.

SOM Table S1

List of P^3 and P^4 forming the Western European Holocene human sample (HH) used in the comparative analyses.

	UP3	UP4	References
Neolithic	Gurgy Les Noisats (GLN04-201, GLN04-277, GLN06-215B, GLN06-215B3, GLN05-308), Mykolas cave (LBGM10)	Gurgy Les Noisats (GLN04-201, GLN04-277, GLN05-308), Mykolas cave (LBGM10-5)	Le Luyer, 2016
Roman Empire	Bosco Pontini (BP 5, BP 6, BP 7)	Bosco Pontini (BP 5, BP 6, BP 7, BP 8, BP 9)	original data
19th-20th centuries	France and Italy (4)	France and Italy (2)	original data

SOM Table S2

List of P^3 and P^4 forming the Neanderthal (NEA) and Western European Holocene human (HH) samples investigated for the presence of a dentine depression on the mesial root aspect.

	P^3	P^4	References
NEA	Krapina (D38, D39, D43, D45, D48, D51, D53, D54, D55, D116), Biache-Saint-Vaast 1 (both UP3s)	Krapina (D40, D41, D42, D44, D46, D47, D49), Scladina (Scla 4A-2/P^4)	Rougier, 2003; Toussaint, 2014; Nespos Database, 2019
HH	*n* = 28	*n* = 20	Le Luyer, 2016; original data